DOI: 10.13009/EUCASS2022-7272
9TH EUROPEAN CONFERENCE FOR AERONAUTICS AND SPACE SCIENCES (EUCASS)

Temperature-dependent Optimized Calibration of a MEMS Inertial Measurement Unit

Eden Meirovich, Daniel Choukroun
Mechanical Engineering Department
Ben-Gurion University of the Negev, Beer-Sheva, 84105, Israel
danielch@bgu.ac.il, meirovicheden@gmail.com

Abstract

This paper is concerned with the temperature-dependent calibration of MEMS inertial measurement units (IMU). The IMU output errors depend on the angular rates, the linear accelerations, and the temperature inputs to the device. Previous works emphasized the development of estimators for *given* inputs, from least-squares batch estimators to Kalman filters or artificial neural networks. Our work focus on optimizing these inputs, either their time profiles or their probability distributions. Several maximization problems of the observability Gramian determinant or trace are proposed with constraints that are derived from operational limitations. Three approaches are deterministic. The first two are parametric where the input profiles are low-order time polynomials, or step and ramp functions with optimized switching times. A third approach is nonparametric and relies on time discretization of the input functions. A fourth approach is probabilistic and seeks the best joint distributions of the temperature and rates. The design approaches are first verified on a single gyro model before being applied to the three-axes gyroscope case. The design model includes biases, scale factors non-linearity of order 4 in the angular rate, and misalignment parameters. All parameters are expressed as third-order temperature polynomials. Profiles of the input temperature and of the angular rates are obtained by merging the randomized and the deterministic nonparametric approach. The sensitivity of the optimized cost is investigated by changing key parameters: the total calibration time, the initial temperature, the sequence of the angular rates, and the time spent at each rate. The method is verified via a simulated calibration with the "best" profiles of the rate and temperature. The method is then validated via an experimental calibration using approximations of the "best" profiles. For the calibration of the accelerometers the input temperature profile is identical to that of the gyroscopes. The performances are compared with calibration results based on "best-practice" profiles of the angular rates and temperature. The proposed approach outperforms the standard one by up to one order of magnitude in the gyroscopes angular rate prediction error. The residual errors are not temperature dependent. A breakdown of the error shows that biases, scale factors, and misalignment contribute evenly.

DOI: 10.13009/EUCASS2022-7272

I. General Problem Formulation

A generic temperature-dependent model of the gyroscope measurement is described as follows:

$$\boldsymbol{\omega}^m = H(\boldsymbol{\omega}, T)\mathbf{x} + \boldsymbol{\epsilon} \tag{1}$$

where
$\boldsymbol{\omega}^m$: 3×1 measured angular velocity vector
$\boldsymbol{\omega}$: 3×1 true angular velocity vector
T: temperature
$\mathbf{x}$: $n \times 1$ vector of constant parameters
$\boldsymbol{\epsilon}$: 3×1 measurement error vector
The components of the vector $\mathbf{x}$ are constant sensitivity parameters. The definition of $\mathbf{x}$ stems from the assumptions on the types of errors and the temperature dependency. Calibration being the estimation of the components of $\mathbf{x}$, given a sequence of rates measurements acquired during a temperature controlled experiment, our objective is to design that experiment in order to enhance the calibration performances. In other words, we seek the time profiles of the rate vector $\boldsymbol{\omega}(t)$ and of the temperature $T(t)$ that will maximize some measure of the calibration performances. Assuming that calibration is performed by a batch Weighted Least-Squares estimator (WLS), natural cost indices are the trace and the determinant of the Observability Gramian, denoted by $M(0,t)$, and defined as follows:

$$M(0,t;\, \boldsymbol{\omega}, T) = \int_0^t H^T(\boldsymbol{\omega}, T) W(\tau) H(\boldsymbol{\omega}, T)\, d\tau \tag{2}$$

where $W(\tau)$ and $H(\boldsymbol{\omega}, T)$ denote the weighting matrix and the measurement matrix at time τ, respectively. In the following, for simplicity, the results are limited to the measurement of a scalar rate, ω, involving scale-factor (S/F), bias, and white noise errors, denoted by β, b, and ϵ, respectively. The measurement design model is thus as follows:

$$\omega^m = \beta(T)\, \omega + b(T) + \epsilon \tag{3}$$

Henceforth, one seeks to maximize either the trace or the determinant of $M(0,t)$ with respect to ω and T, subject to Eq. (3) and to a set of constraints due to experimental limitations:

$$\omega_m \leq \omega \leq \omega_M \tag{4}$$

$$T_m \leq T \leq T_M \tag{5}$$

$$\dot{T}_m \leq \frac{dT}{dt} \leq \dot{T}_M \tag{6}$$

where $\omega_m \leq 0$, $\omega_M \geq 0$, $T_m \leq 0$, $T_M \geq 0$, $\dot{T}_m \leq 0$, $\dot{T}_M \geq 0$. Typically, $\omega_m = -\omega_M = -400[deg/sec]$, $T_m = -30[^oC]$, $T_M = +60[^oC]$, $\dot{T}_m = -2[^oC/mn]$, $\dot{T}_M = +5[^oC/mn]$. As is usually done, the noise is assumed to be independently identically distributed, which justifies choosing a scalar matrix for the weight W. Henceforth the unweighted Gramian will be used. Furthermore, the white noise element will be omitted in the subsequent measurement models for simplicity, without loss of generality.

DOI: 10.13009/EUCASS2022-7272

II. Parametric Design 1

In this section we consider profiles of ω and T that are polynomials in time. The polynomials coefficients are decision variables in the optimization problem at hand.

A. b is a linear function of T

In the following the bias depends linearly on T and the scale-factor remains temperature-invariant.

$$\begin{aligned}\omega^m &= \beta\,\omega_0 + b \\ &= \beta\,\omega + b_0 + b_1 T \\ &= \begin{bmatrix}\omega & 1 & T\end{bmatrix}\begin{bmatrix}\beta \\ b_0 \\ b_1\end{bmatrix} \\ &= H(\omega, T)\,\mathbf{x}\end{aligned} \tag{7}$$

The calibration parameters are β, b_0, b_1 and the Gramian dimension is 3×3.

Example P3: $\omega = \omega_0$ and $T = \eta\tau$
With the above assumptions on ω and T the measurement matrix has the following expression

$$H = \begin{bmatrix}\omega_0 & 1 & \eta\tau\end{bmatrix} \tag{8}$$

and for the Gramian:

$$M(\omega_0, \eta) = \begin{bmatrix}\omega_0^2 t & \omega_0 t & \frac{1}{2}\,\omega_0 \eta t^2 \\ * & t & \frac{1}{2}\,\eta t^2 \\ * & * & \frac{1}{3}\eta^2 t^3\end{bmatrix} \tag{9}$$

In this case, the trace and determinant of M are as follows:

$$\mathrm{tr}M(\omega_0, \eta) = t\left(\omega_0^2 + \frac{t^2}{3}\eta^2 + 1\right) \tag{10}$$

$$\det M(\omega_0, \eta) = 0 \tag{11}$$

The invariance of ω hampers observability yet, again, maximizing the trace subject to the constraints provides some insight. The equivalent optimization problem is formulated as follows:

$$\max_{\omega_0, \eta}\ \omega_0^2 + \frac{t^2}{3}\eta^2 \tag{12}$$

subject to

$$\omega_m \le \omega_0 \le \omega_M \tag{13}$$

$$T_m \le \eta\tau \le T_M \tag{14}$$

$$\dot{T}_m \le \eta \le \dot{T}_M \tag{15}$$

DOI: 10.13009/EUCASS2022-7272

where the numerical values for the bounds are given as follows:

$$\omega_m = -\omega_M = -200[deg/sec] \tag{16}$$
$$T_m = -T_M = -60[^oC] \tag{17}$$
$$\dot{T}_m = -\dot{T}_M = -0.08[^oC/sec] \tag{18}$$
$$t = 100[sec] \tag{19}$$

Analytical solution:

Following [22, Ch.3], let $L(\omega_0, \eta)$ denote the objective function:

$$L(\omega_0, \eta) = \omega_0^2 + \frac{t^2}{3}\eta^2 \tag{20}$$

The constraints (13) are rewritten as follows:

$$f_1(\omega_0, \eta) = \omega_0 - \omega_M \leq 0 \tag{21}$$
$$f_2(\omega_0, \eta) = -\omega_0 + \omega_m \leq 0 \tag{22}$$

The constraints (15) are rewritten next:

$$f_3(\omega_0, \eta) = \eta - \eta_M \leq 0 \tag{23}$$
$$f_4(\omega_0, \eta) = -\eta + \eta_m \leq 0 \tag{24}$$

where η_m, η_M denote the bounds on η, and the constraints (14) yield a set of constraints rewritten as follows:

$$f_5(\omega_0, \eta) = \eta - T_M/\tau \leq 0 \tag{25}$$
$$f_6(\omega_0, \eta) = -\eta + T_m/\tau \leq 0 \tag{26}$$

where $0 < \tau \leq 100$. For the given numerical values, the intersection of the feasible domains of constraints (23) to (26) can be expressed with only two constraints, which yields the following formulation:

$$\max_{\omega_0, \eta} \omega_0^2 + \frac{t^2}{3}\eta^2 \tag{27}$$
$$s.t. \;\; f_i(\omega_0, \eta) \leq 0 \quad i = 1, 2, 3, 4$$

Let $\mathcal{H}(\omega_0, \eta, \lambda)$, $\lambda \in \mathbb{R}^4$, denote the Lagrangian:

$$\mathcal{H}(\omega_0, \eta, \lambda) = \omega_0^2 + \frac{t^2}{3}\eta^2 + \lambda_1(\omega_0 - \omega_M) + \lambda_2(-\omega_0 + \omega_m) + \lambda_3(\eta - \eta_M) + \lambda_4(-\eta + \eta_m) \tag{28}$$

$$\lambda_i \leq 0 \quad \text{if } f_i = 0 \tag{29}$$
$$\lambda_i = 0 \quad \text{if } f_i < 0 \tag{30}$$

The necessary conditions for maximum are:

$$\frac{\partial \mathcal{H}}{\partial \omega_0} = 2\omega_0 + \lambda_1 - \lambda_2 = 0 \tag{31}$$
$$\frac{\partial \mathcal{H}}{\partial \eta} = \frac{2t^2}{3}\eta + \lambda_3 - \lambda_4 = 0 \tag{32}$$

A simple examination of the constraints and of the contours of constant L yields the following observations:

DOI: 10.13009/EUCASS2022-7272

- If a single constraint is effective at the stationary point it is not a maximum.
- Two constraints at most can be simultaneously effective; namely (f_1, f_3), (f_1, f_4), (f_2, f_3), or (f_2, f_4).
- There exist four points where two constraints can be simultaneously effective.

Henceforth the following discussion for each of the four cases, denoted Case 13, Case 14, Case 23, Case 24, respectively.

Case 13:

In this case, constraints (21) and (23) are effective, i.e.

$$\omega_0 = \omega_M \tag{33}$$

$$\eta = \eta_M \tag{34}$$

Using (33),(34) into (31),(32) yields

$$\lambda_1 = -2\,\omega_M \leq 0 \tag{35}$$

$$\lambda_3 = -\frac{2t^2}{3}\eta_M \leq 0 \tag{36}$$

and the optimal cost function L_{13} is:

$$L_{13} = \omega_M^2 + \frac{t^2}{3}\eta_M^2 \tag{37}$$

Note that the simultaneous effective constraints completely define the stationary point. The sufficient conditions for maximum can not be applied since there is no possible variations of L about the stationary point while keeping both constraints effective. The other three cases can be similarly handled. For brevity the developments are omitted and the results are summarized in Table II.A. The global maximum is thus obtained by

CASE	13	14	23	24
ω_0	ω_M	ω_M	ω_m	ω_m
η	η_M	η_m	η_M	η_m
λ_1	$-2\,\omega_M$	$-2\,\omega_M$	0	0
λ_2	0	0	$2\,\omega_m$	$2\,\omega_m$
λ_3	$-\frac{2t^2}{3}\eta_M$	0	$-\frac{2t^2}{3}\eta_M$	0
λ_4	0	$\frac{2t^2}{3}\eta_m$	0	$\frac{2t^2}{3}\eta_m$
L	$\omega_M^2 + \frac{t^2}{3}\eta_M^2$	$\omega_M^2 + \frac{t^2}{3}\eta_m^2$	$\omega_m^2 + \frac{t^2}{3}\eta_M^2$	$\omega_m^2 + \frac{t^2}{3}\eta_m^2$

Table 1.

comparing the values of L at the various stationary points. Recalling the given numerical values,

$$\omega_m = -200[deg/sec] \tag{38}$$

$$\omega_M = 200[deg/sec] \tag{39}$$

$$\eta_m = -0.08[^oC/sec] \tag{40}$$

$$\eta_M = 0.08[^oC/sec] \tag{41}$$

DOI: 10.13009/EUCASS2022-7272

it becomes clear that there are four points with the same maximum value of the cost.

Numerical solution: For the sake of verification of the analytical solution, a numerical solution of (12) was sought. For that purpose a time discretization with step of one second was applied to the constraints (23) to (26). All constraints were inserted in the formulation and the solution was obtained using the Matlab *fmincon Active Set algorithm*. Care was taken in choosing the initial guesses in order to obtain a complete view of the convergence map. Table II.A provides samples of initial guesses along with the solutions. Note that all four solutions of the analytical study were found and that the origin is obviously a fixed point of the algorithm, allbeit as a minimum. Figures 1,2 depict the cost, the contour lines of constant cost, the four optima, and one optimal solution obtained from the initial guess $\omega_0 = 0.1[deg/s]$, $\eta = 0.05[^o/s]$.

Concluding remark: in this example the angular rate should be maintained constant

	Start	End	Start	End	Start	End	Start	End
$\omega_0[\frac{deg}{sec}]$	0.1	200	-0.1	-200	0.1	200	-0.1	-200
$\eta[\frac{^oC}{sec}]$	0.05	0.08	0.05	0.08	-0.05	-0.08	-0.05	-0.08

Table 2.

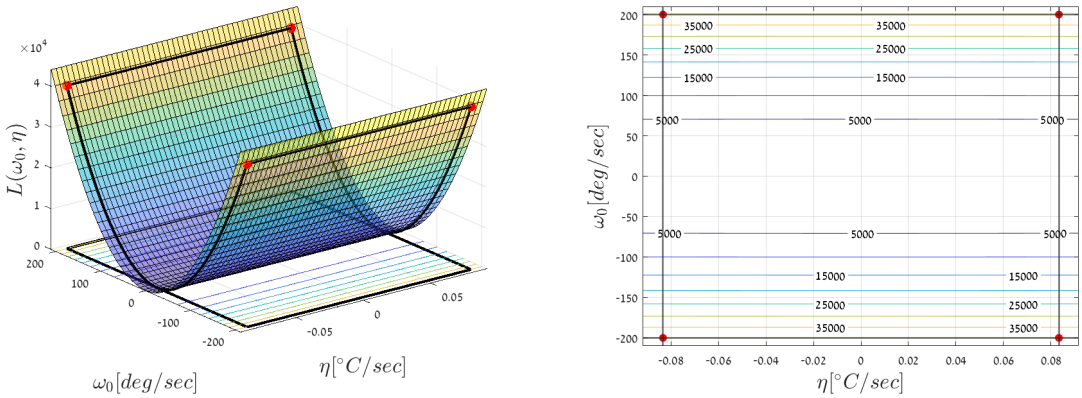

Figure 1. Example P3. The four optima appear as red spots. Contours of constant cost appear almost horizontal due to the high eccentricity of the ellipses.

at one of its bounds, and the temperature should be increased or decreased using the bounds on the temperature rate.

III. Non-parametric Design

In the non-parametric approach the time-varying functions ω and T are generic.

DOI: 10.13009/EUCASS2022-7272

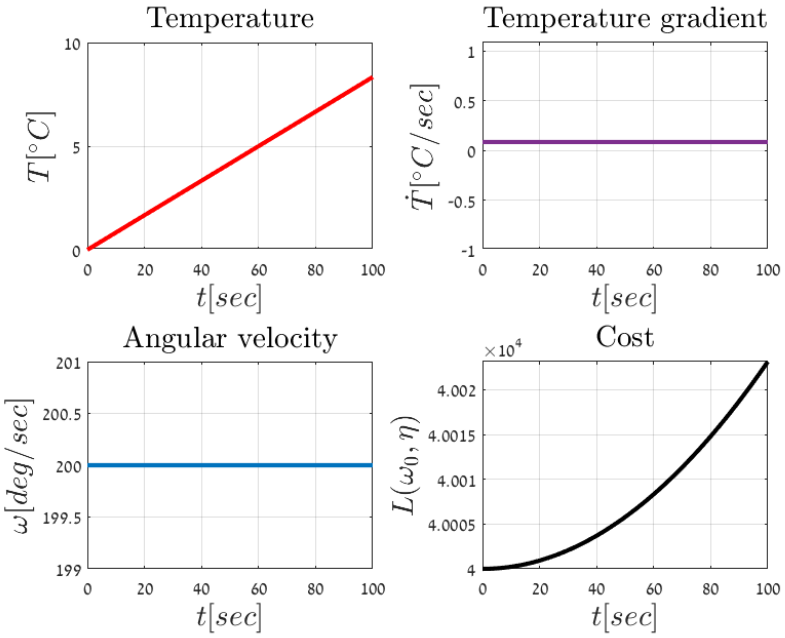

Figure 2. Example P3. The optimal solution $\omega_0 = 200[deg/s]$, $\eta = 0.08[^oC/s]$.

Example NP5: $\beta = \beta_0 + \beta_1 T + \beta_2 T^2 + \beta_3 T^3$ **and** $b = b_0 + b_1 T + b_2 T^2 + b_3 T^3$
In this example, the bias and the scale-factor are polynomials of order three in T, i.e.

$$\begin{aligned}
\omega^m &= \beta\,\omega + b \\
&= (\beta_0 + \beta_1 T + \beta_2 T^2 + \beta_3 T^3)\,\omega + (b_0 + b_1 T + b_2 T^2 + b_3 T^3) \\
&= \begin{bmatrix} \omega & \omega T & \omega T^2 & \omega T^3 & 1 & T & T^2 & T^3 \end{bmatrix} \begin{bmatrix} \beta_0 \\ \beta_1 \\ \beta_2 \\ \beta_3 \\ b_0 \\ b_1 \\ b_2 \\ b_3 \end{bmatrix} \\
&= H(\omega, T)\,\mathbf{x}
\end{aligned} \tag{42}$$

As a result the expression for the Gramian is as follows:

$$M(\omega, T) = t \begin{bmatrix} \overline{\omega^2} & \overline{\omega^2 T} & \overline{\omega^2 T^2} & \overline{\omega^2 T^3} & \overline{\omega} & \overline{\omega T} & \overline{\omega T^2} & \overline{\omega T^3} \\ * & \overline{\omega^2 T^2} & \overline{\omega^2 T^3} & \overline{\omega^2 T^4} & \overline{\omega T} & \overline{\omega T^2} & \overline{\omega T^3} & \overline{\omega T^4} \\ * & * & \overline{\omega^2 T^4} & \overline{\omega^2 T^5} & \overline{\omega T^2} & \overline{\omega T^3} & \overline{\omega T^4} & \overline{\omega T^5} \\ * & * & * & \overline{\omega^2 T^6} & \overline{\omega T^3} & \overline{\omega T^4} & \overline{\omega T^5} & \overline{\omega T^6} \\ * & * & * & * & 1 & \overline{T} & \overline{T^2} & \overline{T^3} \\ * & * & * & * & * & \overline{T^2} & \overline{T^3} & \overline{T^4} \\ * & * & * & * & * & * & \overline{T^4} & \overline{T^5} \\ * & * & * & * & * & * & * & \overline{T^6} \end{bmatrix} \tag{43}$$

DOI: 10.13009/EUCASS2022-7272

The Gramian's expression is simplified as follows:

$$M(\omega,T) = t\begin{bmatrix} \overline{\omega^2} & \overline{\omega^2 T} & \overline{\omega^2 T^2} & \overline{\omega^2 T^3} & 0 & 0 & 0 & 0 \\ * & \overline{\omega^2 T^2} & \overline{\omega^2 T^3} & \overline{\omega^2 T^4} & 0 & 0 & 0 & 0 \\ * & * & \overline{\omega^2 T^4} & \overline{\omega^2 T^5} & 0 & 0 & 0 & 0 \\ * & * & * & \overline{\omega^2 T^6} & 0 & 0 & 0 & 0 \\ * & * & * & * & 1 & \overline{T} & \overline{T^2} & \overline{T^3} \\ * & * & * & * & * & \overline{T^2} & \overline{T^3} & \overline{T^4} \\ * & * & * & * & * & * & \overline{T^4} & \overline{T^5} \\ * & * & * & * & * & * & * & \overline{T^6} \end{bmatrix}$$

$$= t\begin{bmatrix} \overline{\omega^2} & 0 \\ * & 1 \end{bmatrix} \otimes \begin{bmatrix} 1 & \overline{T} & \overline{T^2} & \overline{T^3} \\ * & \overline{T^2} & \overline{T^3} & \overline{T^4} \\ * & * & \overline{T^4} & \overline{T^5} \\ * & * & * & \overline{T^6} \end{bmatrix} \tag{44}$$

which lends itself to the following determinant expression:

$$\det M(\omega,T) = t^8 \overline{\omega^2} \left(\det \begin{bmatrix} 1 & \overline{T} & \overline{T^2} & \overline{T^3} \\ * & \overline{T^2} & \overline{T^3} & \overline{T^4} \\ * & * & \overline{T^4} & \overline{T^5} \\ * & * & * & \overline{T^6} \end{bmatrix} \right) \tag{45}$$

Numerical solution: The functions ω and T are approximated by step functions over a regular time partition of step Δt. Let ω_k and T_k denote the sequences of the angular rate and of the temperature values, respectively, for $k = 1, \ldots, N$, where

$$N = \frac{t}{\Delta t} \tag{46}$$

The optimization variables are the components of the $2N \times 1$ vector $\mathbf{u}$:

$$\mathbf{u} = (\omega_1, \omega_2, \ldots, \omega_N, T_1, T_2, \ldots, T_N) \tag{47}$$

The constraints over $\mathbf{u}$ are derived from (4), (5), (6) as follows. For the angular rate, (4) yields

$$f_{1,k}(\mathbf{u}) = \omega_k - \omega_M \leq 0 \quad k = 1, \ldots N \tag{48}$$

$$f_{2,k}(\mathbf{u}) = -\omega_k + \omega_m \leq 0 \quad k = 1, \ldots N \tag{49}$$

For the temperature, (5) yields

$$f_{3,k}(\mathbf{u}) = T_k - T_M \leq 0 \quad k = 1, \ldots N \tag{50}$$

$$f_{4,k}(\mathbf{u}) = -T_k + T_m \leq 0 \quad k = 1, \ldots N \tag{51}$$

and the constraint on the temperature gradient, (6), is discretized via the first-order forward difference formula,

$$\frac{dT}{dt} = \frac{T_{k+1} - T_k}{\Delta t} \tag{52}$$

DOI: 10.13009/EUCASS2022-7272

which yields the following additional set of constraints:

$$f_{5,k}(\mathbf{u}) = T_{k+1} - T_k - \dot{T}_M \leq 0 \quad k = 1, \dots N \tag{53}$$

$$f_{6,k}(\mathbf{u}) = T_k - T_{k+1} + \dot{T}_m \leq 0 \quad k = 1, \dots N \tag{54}$$

In total, there are $6N - 2$ constraints for $2N$ optimization variables. In general, a discussion on the minimal feasibility domain should be made, which depends on the values of the bounds. The problem parameters shall admit the following values for the sake of this example:

$$\omega_m = -\omega_M = -200[\frac{deg}{sec}] \tag{55}$$

$$T_m = -T_M = -60[^oC] \tag{56}$$

$$\dot{T}_m = -\dot{T}_M = -5[\frac{^oC}{mn}] \tag{57}$$

$$t = 100[min] \tag{58}$$

The results are summarized in Fig. 3. Each row of graphs illustrates the optimal solution upon convergence from different initial guesses of ω and T. The first two initial guesses were drawn at random from uniform distributions while the third initial guesses were chosen as linear functions of time spanning the whole ranges of feasible values.

Concluding remark: The optimization algorithm converges to different profiles emphasizing the multiplicity of optimal solutions and the room for further constraints in shaping the time profiles of ω and T. It is a remarkable result that a few values of ω and T are featured in the optimal solutions without additional constraints. This is illustrated by the plots of the sample joint distributions built from the optimal solutions. The three distributions show eight peaks with very similar levels and at very close locations in the sample space (ω, T). Notice that these empirical distributions are nearly symmetrical around the means of the marginal distributions. This result further motivates the formulation of the optimization problem on probabilistic grounds.

IV. Parametric Design 2

The parametric approach using time polynomials is straightforward and provides some insights on the optimization problem at hand. Yet it has two drawbacks: 1) it is impractical for high-order polynomials since following such profiles would be cumbersome from the operator's point of view. 2) the time-discretization yields a large amount of constraints, hindering analytical insights into the problem. The nonparametric approach is more general and yields higher values for the cost. Yet the purely numerical approach isn't insightful and yields impractical profiles as-is. In this section we consider profiles of piecewise-constant (PWC) functions of time for ω and PWC or piecewise-linear (PWL) functions for T. That is indeed a standard approach of designing time profiles of ω and T in a calibration experiment. Yet the steps levels and the time epochs of the switches become in our approach decision variables for the optimization problem. Henceforth, instead of apriori arbitrary discretized timeline and step-levels, the optimization solution will provide sufficient ones. Further, the number of constraints is set upfront as it depends on the number of levels in ω.

Example SP5: $\beta = \beta_0 + \beta_1 T + \beta_2 T^2 + \beta_3 T^3$ **and** $b = b_0 + b_1 T + b_2 T^2 + b_3 T^3$
Consider the same model as in Example NP5 where β and b are cubic functions of T.

DOI: 10.13009/EUCASS2022-7272

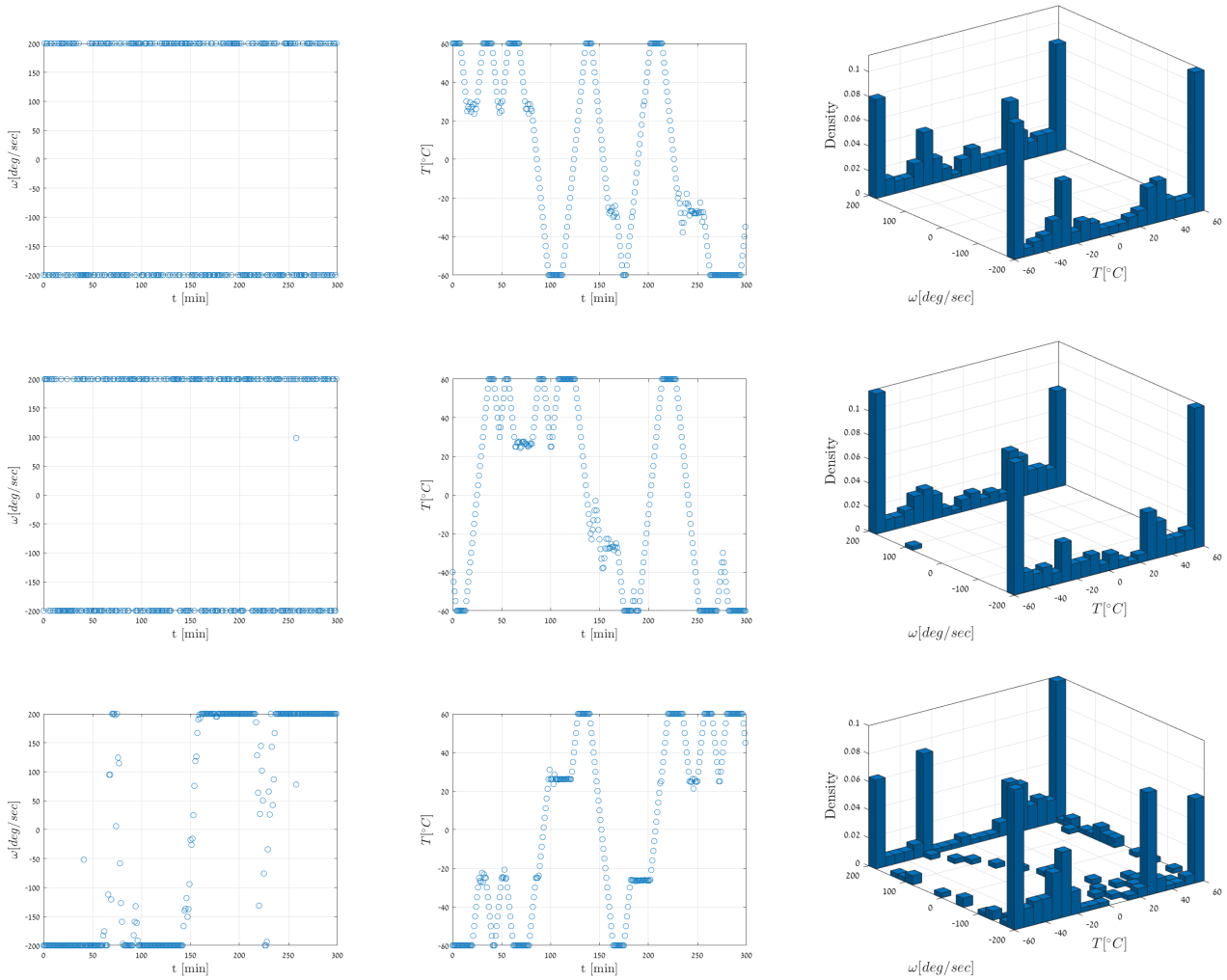

Figure 3. Example NP5. Optimal time profiles for ω and T. The joint sample distributions depict eight similar peaks at the same locations.

Then the eight-dimensional Gramian has the expression in (43). Figure 4 shows the optimal profiles for ω and T, and the associated sample joint distribution. The optimal profile for ω features only two levels $\pm 200 \frac{deg}{sec}$ of seven visible steps. The optimal profile of T features four levels $\{\pm 60^o C, \pm 27^o C\}$ distributed over nine steps. The sample joint distribution of ω, T is identical to that of Example NP5. The cumulative time duration at each ω and T-level are identical. Hence this example verifies the result from NP5.

V. Randomized Design

A. Problem Formulation

In the randomized design approach, the angular rate and the temperature are modeled as random parameters rather than deterministic functions of time. The motivation for this approach is twofold: 1) a fairly general idea is that randomization enlarges the search space and might yield higher values of the cost index, 2) results from the nonparametric

DOI: 10.13009/EUCASS2022-7272

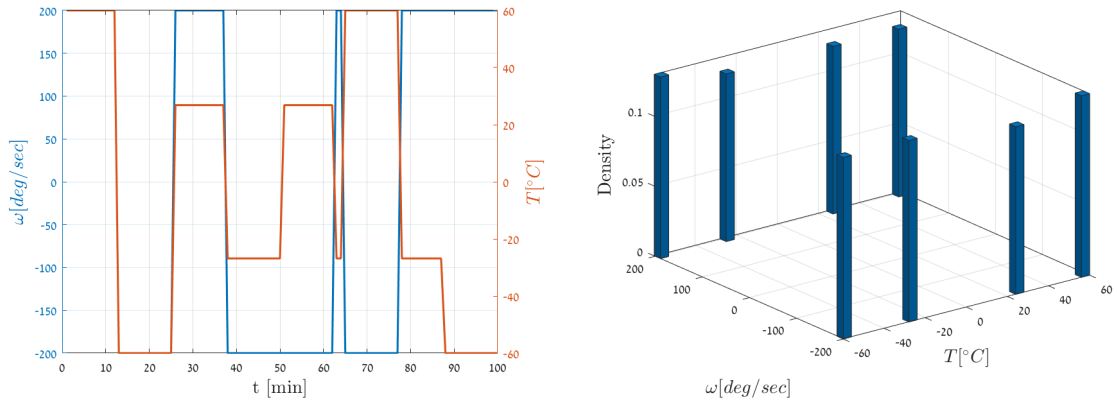

Figure 4. Example SP5. Optimal time profiles for ω and T. The joint distribution has eight uniform peaks.

and step-parametric approaches highlight the particular statistical distributions of the ω-samples and of the T-samples, 3) the order of the ω^m measurements with respect to time is irrelevant to the optimal value of the batch LS cost. Consider the results from Example NP5 for instance, see Fig. 3. The graphs of ω suggest that the angular rate input to the calibration should be set at $\pm 200\,[\frac{deg}{sec}]$ with equal proportions in time, i.e. in the number of measurement samples. Since the order of the measurement is irrelevant to the value of the LS cost, we may consider ω as a random variable and seek its best distribution. Indeed we consider ω, T as a random vector and seek its best joint distribution. The general problem formulation needs therefore to be modified as explained next. Consider the generic temperature-dependent model of the gyroscope measurement (1)

$$\omega^m = H(\mathbf{y})\mathbf{x} + \epsilon \tag{59}$$

where $\mathbf{y} = (\omega, T)$ denotes the vector of random design parameters, $\mathbf{x} \in \mathbb{R}^n$ and ϵ is a zero-mean white Gaussian noise with intensity $R = \sigma_\epsilon^2$. Let Ω_y be the set of allowable values, as given in (4) and (5):

$$\omega_m \leq \omega \leq \omega_M \tag{60}$$

$$T_m \leq T \leq T_M \tag{61}$$

The constraints on the temperature gradient is not taken into account as the model is assumed to be independent of $\dot{T}$, and T is not modeled as a random process. The set Ω_y is a closed and compact set. Let q denote a probability measure for all Borel sets of Ω_y, including single points, i.e. combinations of single values for ω and T within the feasible set. Let $M(y)$ denote the elementary Gramian corresponding to any single-point realization y of $\mathbf{y}$, i.e.

$$M(y) = [H(y)]^T H(y) \tag{62}$$

Let $M(q)$ denote the expectation of $M(\mathbf{y})$ for a given distribution q, i.e.

$$M(q) = E\{M(\mathbf{y})\} = \int_{y \in \Omega_y} M(y) q(dy) \tag{63}$$

DOI: 10.13009/EUCASS2022-7272

We seek an optimal design q^* that maximizes the determinant of the expected value of $M(q)$:

$$\max_q \left[\det M(q)\right]$$
$$\text{subject to} \int_{\Omega_y} q(dy) = 1, \quad 0 \leq q(dy) \leq 1 \tag{64}$$

The set of all matrices $M(q)$ is a closed and convex set in $\mathbb{R}^{\frac{n(n+1)}{2}+1}$. It is the convex hull of elementary Gramians $M(y)$, so that there exists a discrete probability distribution that satisfies the following equality:

$$M(q) = \sum_{i=1}^{k} q_i M(y_i), \quad 0 \leq q_i \leq 1, \quad \sum_{i=1}^{k} q_i = 1 \tag{65}$$

where $k \leq \frac{n(n+1)}{2} + 1$. The following theorem summarizes key properties of the optimal design q^*, which are used in the numerical iterative algorithm that follows.
Theorem:
Any optimal design q^* satisfies the three following equivalent properties

1. q^* maximizes $\det M(q)$
2. q^* minimizes $\max_{y\in\Omega_y} \operatorname{tr}\left[M^{-1}(q)M(y)\right]$
3. $\max_{y\in\Omega_y} \operatorname{tr}\left[M^{-1}(q^*)M(y)\right] = n$

All designs that satisfy the above properties share the same expected Gramian $M(q)$, as do their convex combinations.
Algorithm:

1. Start with an initial guess q^0 such that $M(q^0)$ is nonsingular.
2. At every iteration j: find the maximum of $\operatorname{tr}\left[M^{-1}(q^j)M(y)\right]$ for all $y \in \Omega_y$ and its maximizer y_j
3. If $\operatorname{tr}\left[M^{-1}(q^j)M(y_j)\right] = n$ stop, otherwise set

$$q^{j+1} = (1-\alpha_j)q^j + \alpha_j q(y_j) \tag{66}$$

and choose $0 \leq \alpha_j \leq 1$ by solving

$$\max_{\alpha_j} \det M[q^{j+1}] \tag{67}$$

The result is a discrete probability distribution q^* with support of at most $\frac{n(n+1)}{2}+1$ realizations in the sample space of (ω, T). In practice this number is even less as will be shown in the following examples.

Example R3: $\beta = \beta_0 + \beta_1 T + \beta_2 T^2 + \beta_3 T^3$ **and** $b = b_0 + b_1 T + b_2 T^2 + b_3 T^3$
Consider the same measurement model as in Example NP5. Both the scale factor and the bias are cubic functions of the temperature T. The associated measurement matrix is therefore identical and rewritten here for convenience:

$$H(\omega, T) = \begin{bmatrix} \omega & \omega T & \omega T^2 & \omega T^3 & 1 & T & T^2 & T^3 \end{bmatrix} \tag{68}$$

DOI: 10.13009/EUCASS2022-7272

The expression of the Gramian for any probability distribution q of (ω, T), is as follows

$$M(q) = \begin{bmatrix} \widehat{\omega^2} & \widehat{\omega^2 T} & \widehat{\omega^2 T^2} & \widehat{\omega^2 T^3} & \widehat{\omega} & \widehat{\omega T} & \widehat{\omega T^2} & \widehat{\omega T^3} \\ * & \widehat{\omega^2 T^2} & \widehat{\omega^2 T^3} & \widehat{\omega^2 T^4} & \widehat{\omega T} & \widehat{\omega T^2} & \widehat{\omega T^3} & \widehat{\omega T^4} \\ * & * & \widehat{\omega^2 T^4} & \widehat{\omega^2 T^5} & \widehat{\omega T^2} & \widehat{\omega T^3} & \widehat{\omega T^4} & \widehat{\omega T^5} \\ * & * & * & \widehat{\omega^2 T^6} & \widehat{\omega T^3} & \widehat{\omega T^4} & \widehat{\omega T^5} & \widehat{\omega T^6} \\ * & * & * & * & 1 & \widehat{T} & \widehat{T^2} & \widehat{T^3} \\ * & * & * & * & * & \widehat{T^2} & \widehat{T^3} & \widehat{T^4} \\ * & * & * & * & * & * & \widehat{T^4} & \widehat{T^5} \\ * & * & * & * & * & * & * & \widehat{T^6} \end{bmatrix} \tag{69}$$

where $\widehat{f}$ denote the expectation of f according to q. The values of the bounds of ω and T are provided in Table V.A. Concluding remark: the optimization algorithm and

ω_m	ω_M	T_m	T_M
$-400\,[\frac{deg}{sec}]$	$400\,[\frac{deg}{sec}]$	$-60\,[^oC]$	$60\,[^oC]$

Table 3. Example R3. Bounds parameters.

the related theory are verified in this example. The convergence transient phase lasts about 50 iteration. Starting with different initial guesses still yield the same eight-points uniform discrete distribution. This provides a probabilistic ground to the findings of Example NP5.

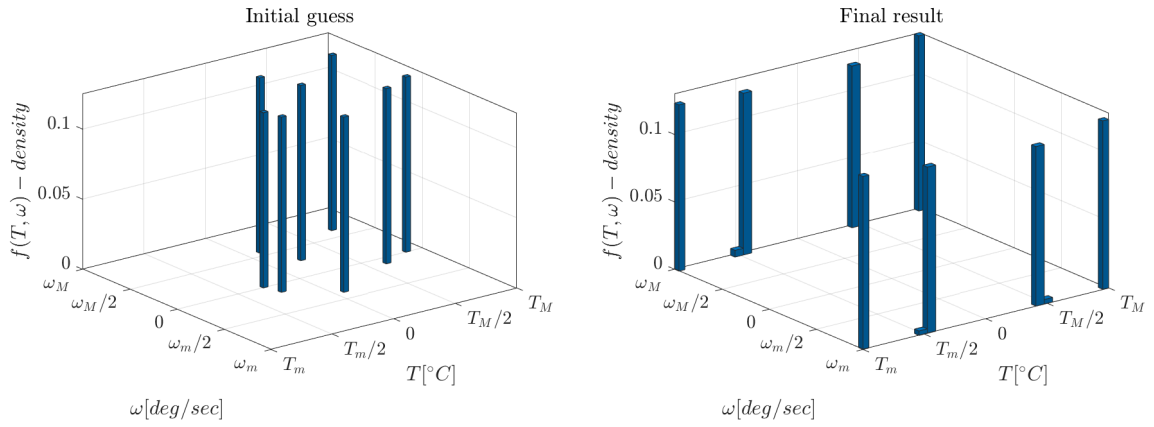

Figure 5. Example R3. Initial guess and optimal solution. The optimal distribution is a uniform eight-points distribution.

B. Concluding remarks

The above results converge in showing a consistent picture of the joint distributions of the angular rates and temperatures. The measurement scheduling is still a missing part of the probabilistic design. The final manuscript will provide feasible time profiles of the gyro rates and temperatures based on the optimization approaches and calibration results from simulated and experimental data. The approach will be extended to a full Inertial Measurement Unit.

DOI: 10.13009/EUCASS2022-7272

$\omega\,[\frac{deg}{sec}]$	$T\,[^oC]$	mass probabilities q_i
-400	-60	$1/8$
-400	-30	$1/8$
-400	30	$1/8$
-400	60	$1/8$
400	-60	$1/8$
400	-30	$1/8$
400	30	$1/8$
400	60	$1/8$

Table 4. Example R3. Optimal distribution.

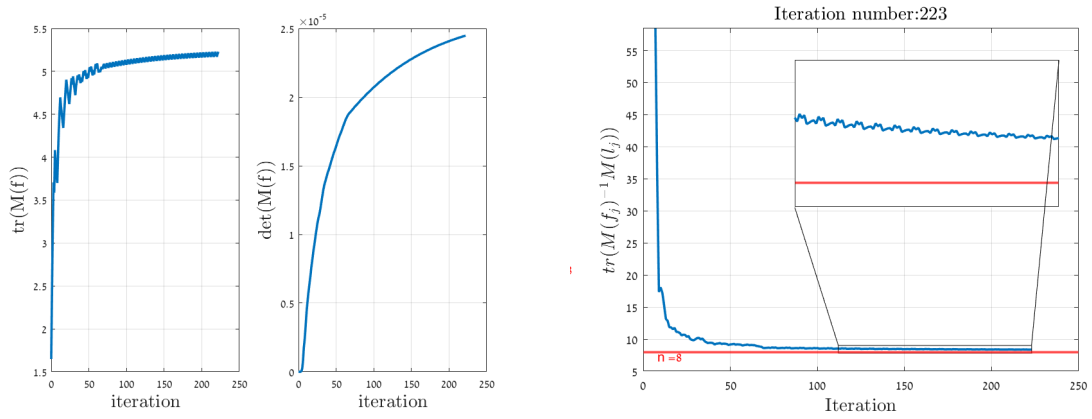

Figure 6. Example R3. Monotonous variations of the cost index and of the optimality index along the iterative process.

VI. Three-axes gyroscopes calibration: simulation and experimentation

A. Best input design

1. Rate measurement design model

The design model for the angular rates measurement of the three-axes gyroscopes is provided as follows:

$$\begin{pmatrix}\omega_x^m\\ \omega_y^m\\ \omega_z^m\end{pmatrix} = \begin{pmatrix}b_x\\ b_y\\ b_z\end{pmatrix} + \begin{bmatrix}\beta_x & \psi_{xy} & \psi_{xz}\\ \psi_{yx} & \beta_y & \psi_{yz}\\ \psi_{zx} & \psi_{zy} & \beta_z\end{bmatrix}\begin{pmatrix}\omega_x\\ \omega_y\\ \omega_z\end{pmatrix} + \begin{pmatrix}d_x\\ d_y\\ d_z\end{pmatrix} + \begin{pmatrix}\epsilon_x\\ \epsilon_y\\ \epsilon_z\end{pmatrix} \tag{70}$$

where
$\omega_x^m, \omega_y^m, \omega_z^m$: measured angular rates
$\omega_x, \omega_y, \omega_z$: true angular rates, equivalent to the table commanded angular rates
b_x, b_y, b_z: biases
$\beta_x, \beta_y, \beta_z$: scale factors (SF) that are independent of $\boldsymbol{\omega}$
ψ_{ij}: misalignment and nonorthogonality (MANO) parameters

DOI: 10.13009/EUCASS2022-7272

d_x, d_y, d_z: scale factors nonlinearity (NL) up to ω^4, i.e.

$$d = \gamma\,\omega^2 + \delta\,\omega^3 + \alpha\,\omega^4 \tag{71}$$

where the axis subscript were dropped for the sake of clarity.
$\epsilon_x, \epsilon_y, \epsilon_z$: independent identically distributed noise terms, $\sigma_\epsilon = 0.01\ deg/sec$.
All the parameters are assumed to vary with the temperature according to a third order polynomial, as follows:

$$b = b_0 + b_1 T + b_2 T^2 + b_3 T^3 \tag{72}$$
$$\beta = \beta_0 + \beta_1 T + \beta_2 T^2 + \beta_3 T^3 \tag{73}$$
$$\psi = m_0 + m_1 T + m_2 T^2 + m_3 T^3 \tag{74}$$
$$\gamma = \gamma_0 + \gamma_1 T + \gamma_2 T^2 + \gamma_3 T^3 \tag{75}$$
$$\delta = \delta_0 + \delta_1 T + \delta_2 T^2 + \delta_3 T^3 \tag{76}$$
$$\alpha = \alpha_0 + \alpha_1 T + \alpha_2 T^2 + \alpha_3 T^3 \tag{77}$$

The 84×1 vector of parameters is defined as follows:

$$x = \Big[x_x\, x_y\, x_z\Big]^T_{84\times 1} \tag{78}$$

$$x_x = \Big[b_{x0}\, b_{x1}\, b_{x2}\, b_{x3}\, \beta_{x0}\, \beta_{x1}\, \beta_{x2}\, \beta_{x3}\, \gamma_{x0}\, \gamma_{x1}\, \gamma_{x2}\, \gamma_{x3}\, \delta_{x0}\, \delta_{x1}\, \delta_{x2}\, \delta_{x3}\, \alpha_{x0}\, \alpha_{x1}\, \alpha_{x2}\, \alpha_{x3}\, m_{xy0}\, m_{xy1}\, m_{xy2}\, m_{xy3}\, m_{xz0}\, m_{xz1}\, m_{xz2}\, m_{xz3}\Big]^T_{28\times 1}$$
$$x_y = \Big[b_{y0}\, b_{y1}\, b_{y2}\, b_{y3}\, \beta_{y0}\, \beta_{y1}\, \beta_{y2}\, \beta_{y3}\, \gamma_{y0}\, \gamma_{y1}\, \gamma_{y2}\, \gamma_{y3}\, \delta_{y0}\, \delta_{y1}\, \delta_{y2}\, \delta_{y3}\, \alpha_{y0}\, \alpha_{y1}\, \alpha_{y2}\, \alpha_{y3}\, m_{yx0}\, m_{yx1}\, m_{yx2}\, m_{yx3}\, m_{yz0}\, m_{yz1}\, m_{yz2}\, m_{yz3}\Big]^T_{28\times 1}$$
$$x_z = \Big[b_{z0}\, b_{z1}\, b_{z2}\, b_{z3}\, \beta_{z0}\, \beta_{z1}\, \beta_{z2}\, \beta_{z3}\, \gamma_{z0}\, \gamma_{z1}\, \gamma_{z2}\, \gamma_{z3}\, \delta_{z0}\, \delta_{z1}\, \delta_{z2}\, \delta_{z3}\, \alpha_{z0}\, \alpha_{z1}\, \alpha_{z2}\, \alpha_{z3}\, m_{zx0}\, m_{zx1}\, m_{zx2}\, m_{zx3}\, m_{zy0}\, m_{zy1}\, m_{zy2}\, m_{zy3}\Big]^T_{28\times 1}$$

Hence the measurement matrix is expressed as follows:

$$H(\omega_x, \omega_y, \omega_z, T) = \begin{bmatrix} h_x & 0_{1\times 28} & 0_{1\times 28} \\ 0_{1\times 28} & h_y & 0_{1\times 28} \\ 0_{1\times 28} & 0_{1\times 28} & h_z \end{bmatrix}_{3\times 84} \tag{79}$$

where

$$h_x = \Big[1\, T\, T^2\, T^3\, \omega_x\, \omega_x T\, \omega_x T^2\, \omega_x T^3\, \omega_x^2\, \omega_x^2 T\, \omega_x^2 T^2\, \omega_x^2 T^3\, \omega_x^3\, \omega_x^3 T\, \omega_x^3 T^2\, \omega_x^3 T^3\, \omega_x^4\, \omega_x^4 T\, \omega_x^4 T^2\, \omega_x^4 T^3\, \omega_y\, \omega_y T\, \omega_y T^2\, \omega_y T^3\, \omega_z\, \omega_z T\, \omega_z T^2\, \omega_z T^3\Big]_{1\times 28}$$
$$h_y = \Big[1\, T\, T^2\, T^3\, \omega_y\, \omega_y T\, \omega_y T^2\, \omega_y T^3\, \omega_y^2\, \omega_y^2 T\, \omega_y^2 T^2\, \omega_y^2 T^3\, \omega_y^3\, \omega_y^3 T\, \omega_y^3 T^2\, \omega_y^3 T^3\, \omega_y^4\, \omega_y^4 T\, \omega_y^4 T^2\, \omega_y^4 T^3\, \omega_x\, \omega_x T\, \omega_x T^2\, \omega_x T^3\, \omega_z\, \omega_z T\, \omega_z T^2\, \omega_z T^3\Big]_{1\times 28}$$
$$h_z = \Big[1\, T\, T^2\, T^3\, \omega_z\, \omega_z T\, \omega_z T^2\, \omega_z T^3\, \omega_z^2\, \omega_z^2 T\, \omega_z^2 T^2\, \omega_z^2 T^3\, \omega_z^3\, \omega_z^3 T\, \omega_z^3 T^2\, \omega_z^3 T^3\, \omega_z^4\, \omega_z^4 T\, \omega_z^4 T^2\, \omega_z^4 T^3\, \omega_x\, \omega_x T\, \omega_x T^2\, \omega_x T^3\, \omega_y\, \omega_y T\, \omega_y T^2\, \omega_y T^3\Big]_{1\times 28}$$

There are 28 parameters per axis, hence 84 parameters for the three axes. The measurement sampling time and the final time are as follows:

$$\Delta t = 1\ \text{sec}, \qquad t_f = 4\ \text{h} = 240\ \text{mn} \tag{80}$$

2. Best temperature and rates profiles

The randomized approach was first implemented. The problem of maximizing the determinant of the expected value of the observability Gramian was solved subject to:

$$-400\frac{deg}{sec} \leq \omega \leq 400\frac{deg}{sec} \tag{81}$$
$$-60\,^oC \leq T \leq 60\,^oC \tag{82}$$

DOI: 10.13009/EUCASS2022-7272

where ω denotes ω_x, ω_y, and ω_z. There are additional constraints on the rates in the three dimensional case. Given that the calibration table rotates around a single axis at a given time, only a single component of the angular velocity vector can be non-zero at that same time. This mutually exclusive condition is inserted in the probability density function (PDF) seeking algorithm. The results are shown in Fig. 7 in terms of the two-dimensional PDF in ω and T, one per axis.

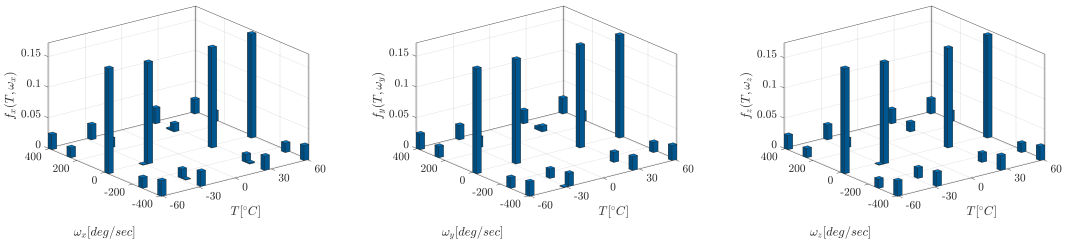

Figure 7. Probability density functions in ω and T.

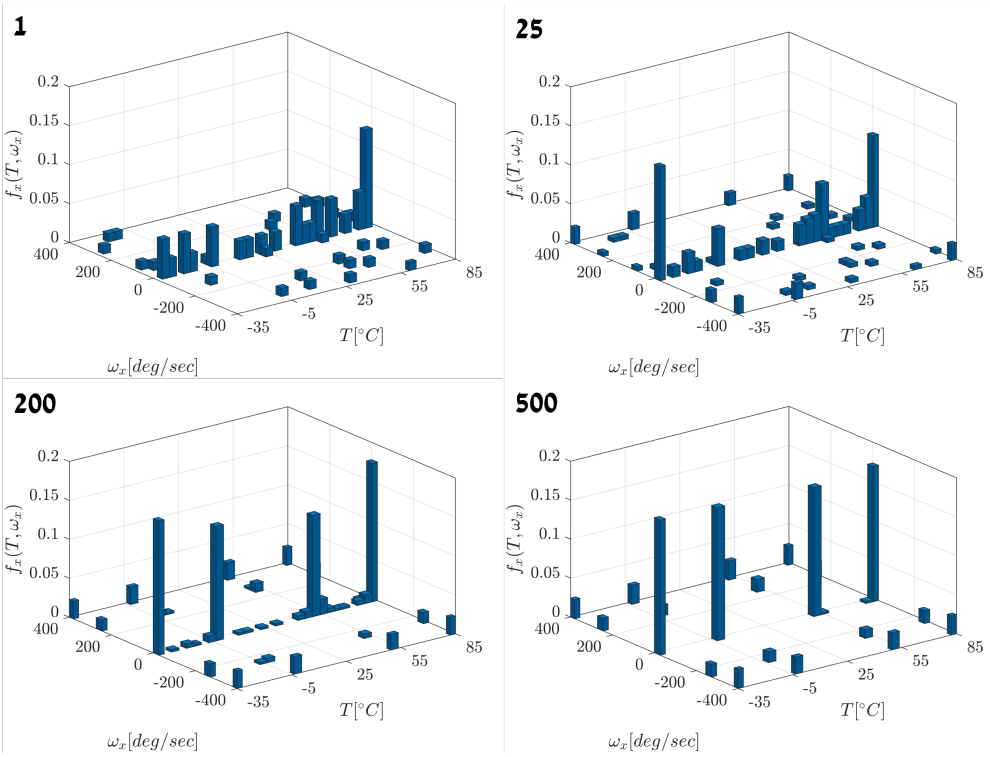

Figure 8. Algorithem results: iteration 1,25,200 and 500.

These PDFs are obtained by simply integrating the four-dimensional PDF along the appropriate dimensions. Notice the larger peaks about the zero value for the rates. That is a direct consequence of the mutually exclusive constraints explained above. Except for the zero rates, the optimized distributions are concentrated at sixteen discrete locations, where T and ω take on the values described in Table VI.A.2. This profile indicates the best values at which the angular rate should be measured and the best levels of temperatures at which the rates should be samples. Yet this solution is not practical

DOI: 10.13009/EUCASS2022-7272

per se since it would require instantaneous “jumps" from one temperature to another. A second step in the design consists in implementing the deterministic nonparametric approach. The problem of maximizing the Gramian determinant was solved subject to additional constraints on the temperature rate:

$$-400\frac{deg}{sec} \leq \omega \leq 400\frac{deg}{sec} \tag{83}$$

$$-35\,^oC \leq T \leq 85\,^oC \tag{84}$$

$$0.5\,\frac{^oC}{mn} \leq \frac{dT}{dt} \leq 2\,\frac{^oC}{mn}, \quad \text{if } \tau \leq 120\,mn \tag{85}$$

$$-0.5\,\frac{^oC}{mn} \leq \frac{dT}{dt} \leq -2\,\frac{^oC}{mn}, \quad \text{if } 120\,mn \leq \tau \leq 240\,mn \tag{86}$$

$\omega\,[\frac{deg}{sec}]$	$T\,[^oC]$	mass probabilities q_i
-400	-60	$5/200$
-400	-30	$5/200$
-400	30	$5/200$
-400	60	$5/200$
-240	-60	$3/200$
-240	-30	$3/200$
-240	30	$3/200$
-240	60	$3/200$
240	-60	$3/200$
240	-30	$3/200$
240	30	$3/200$
240	60	$3/200$
400	-60	$5/200$
400	-30	$5/200$
400	30	$5/200$
400	60	$5/200$
0	60	$1/6$
0	30	$1/6$
0	-30	$1/6$
0	-60	$1/6$

Table 5. Optimal sampling values for ω, T. per axis.

The sought profile of T is provided in Fig. 9. The nominal profile for T is the blue line. The nominal profile for ω is provided in the right-hand-side of the Figure. Its pattern is empirical, yet it stems from the operational constraints. The profile of T is intuitive and shows the various “stations" at which the gyro measurement should be acquired.

3. Parameters variation

The proposed profile is suboptimal. This requires verifying the potential loss of performances if some parameters vary. Key parameters in this short study consists of the total

DOI: 10.13009/EUCASS2022-7272

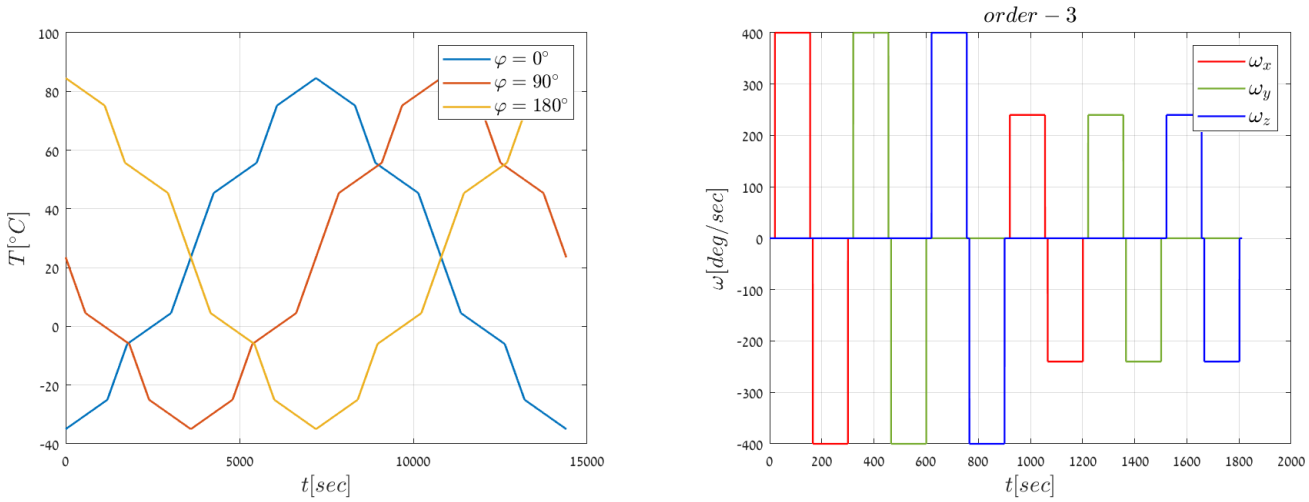

Figure 9. Best profiles of ω and T under constraints.

duration of the calibration, t_f, the number of rounds performed by the table when spinning at the high rate, N_{sp}, the initial temperature, $T(0)$, and the sequence of rates. The decrease in t_f shows that the T-profile shrinks and becomes a simple "tooth" below 120 mn. Increasing the number of rounds spent in a single spin by the table increases the cost

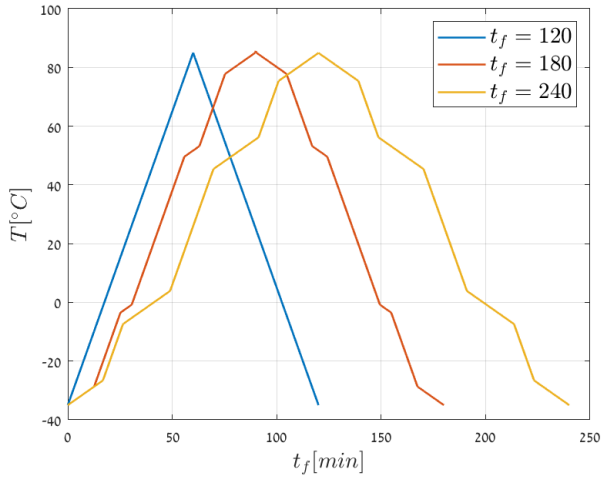

Figure 10. Impact of decreasing the time duration t_f.

function, i.e. the determinant of the Gramian, within a certain range. Figure 11 shows how the cost varies as a function of both t_f and N_{sp}. It appears that increasing t_f beyond 160 minutes and N_{sp} beyond 20 rounds presents no cost improvement. For obvious reasons starting with the initial temperature at room temperature, i.e. $T(0) = 25^oC$, is advantageous. Various cases were tested by varying the initial temperature. The results are shown in Fig. 12. Three temperature profiles are depicted. The same three cases yield the plots in the second graph. It appears that the performances are invariant under changes of initial phase. To conclude one can simply follow the red plot for the T-profile, which starts at the room temperature 25^oC, without impacting the performances.

DOI: 10.13009/EUCASS2022-7272

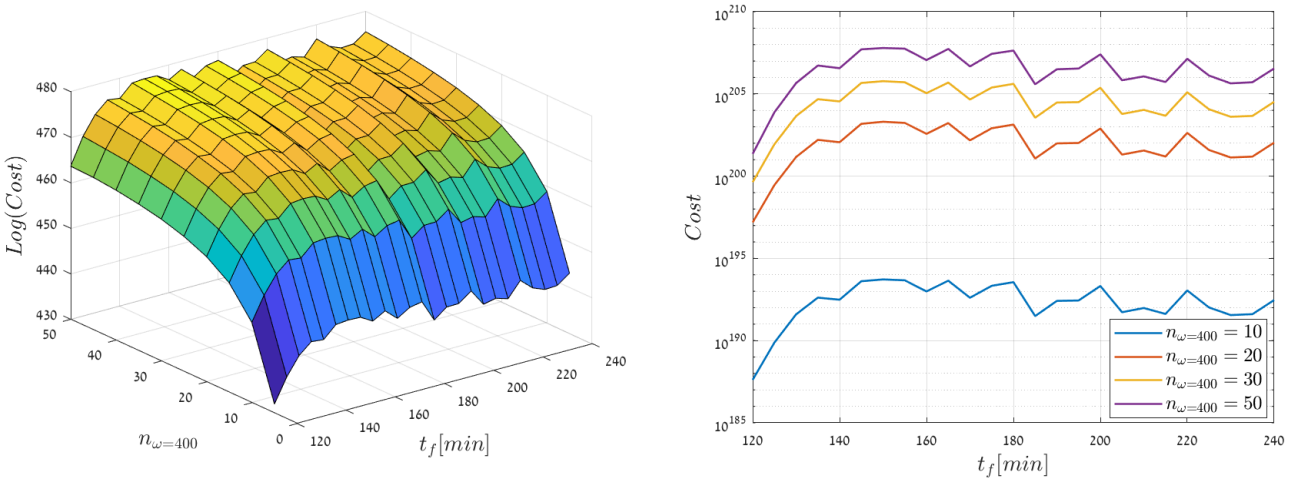

Figure 11. Impact of changing t_f and N_{sp}.

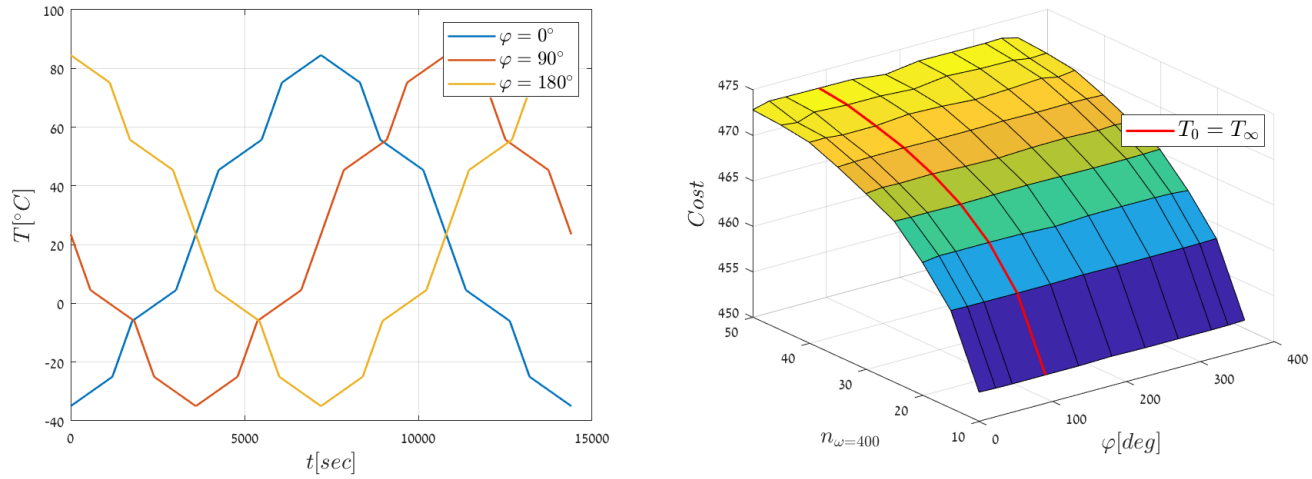

Figure 12. Impact of changing $T(0)$ and N_{sp}.

B. Simulated calibration

1. Rate measurement truth model

The truth model and the design model are identical except for the scale factors nonlinearity:

$$d = \sum_{1}^{4} C_i(T) \cos\left(iK\frac{\omega}{\omega_{FR}}\right) + S_i \sin\left(iK\frac{\omega}{\omega_{FR}}\right) \tag{87}$$

DOI: 10.13009/EUCASS2022-7272

where

$$\omega_{FR} = 400\ deg/sec \tag{88}$$
$$C_1(T) = C_{10} + C_{11}(T - T_0) \tag{89}$$
$$C_2(T) = C_{20} \tag{90}$$
$$C_3(T) = C_{30} \tag{91}$$
$$C_4(T) = C_{40} \tag{92}$$
$$S_1(T) = S_{10} + S_{11}(T - T_0) + S_{12}(T - T_0)^2 \tag{93}$$
$$S_2(T) = S_{20} \tag{94}$$
$$S_3(T) = S_{30} \tag{95}$$
$$S_4(T) = S_{40} \tag{96}$$

The value of the parameters are provided in the Appendix.

2. Calibration methodology

The best input profiles of ω and T are used to produce the measurement matrix for a batch of $N = 14400$ samples per axis, that is 240 minutes at a sampling rate of 1 Hz. The truth model is used to simulate the rate measurements. The proposed measurement profiles for ω and T are depicted in Fig. 15. Notice that the plots of ω include the measurement

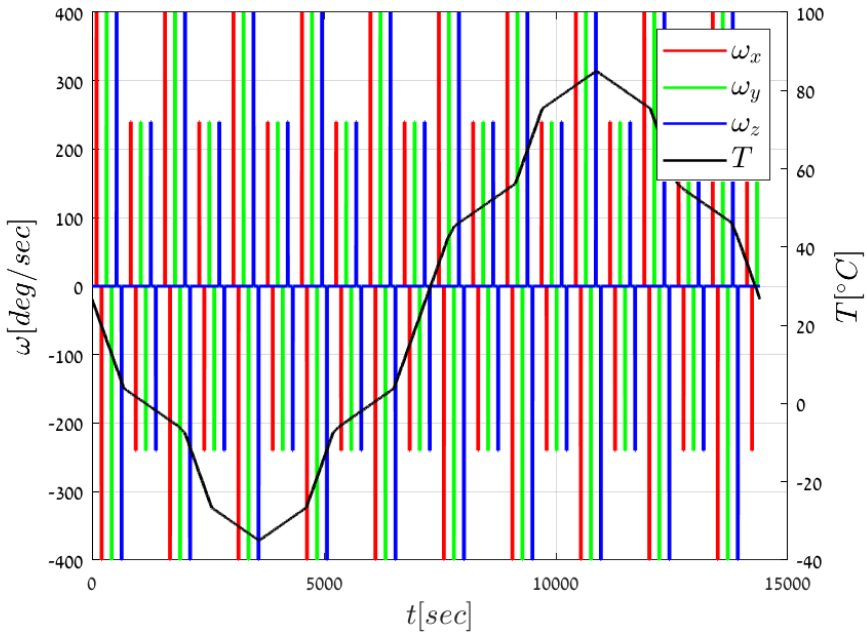

Figure 13. Novel measurement profiles for T and ω.

errors. This batch of rate measurements is used in a Least-Squares estimator to calculate the estimate of the 84×1 vector of parameters $\widehat{\mathbf{x}}$. The estimate $\widehat{\mathbf{x}}$ is used in order to calculate the predicted rate measurements for any sample of the batch. Let $\widetilde{Z}$ denote the $N \times 1$ vector of the measurement residuals, we define the following performance index

DOI: 10.13009/EUCASS2022-7272

per batch:

$$J = \frac{\|\widetilde{Z}\|}{\sqrt{N}} \tag{97}$$

and the following index for N_{MC} batches:

$$J_{MC} = \frac{1}{N_{MC}} \sum_{i=1}^{N_{MC}} J_i \tag{98}$$

where J_i denotes the cost for a single batch. The difference between the batches consists of the sequence of white noise that is generated at random for each batch. When the calculation of the measurement residuals is done over the batch of measurements that is used for the calibration the results are labeled "same set". When a different set of measurements is used, the results are labeled "reference set". We used four different batches of reference measurements in the performance analysis. The reference measurements were generated using particular profiles for ω and T, different from the best profiles. For the sake of comparison with, the calibration process is duplicated using standard profiles of ω and T, labeled "old system". The profiles of the "old system" are depicted next. Figure 20 shows the profile of ω for the reference set 1.

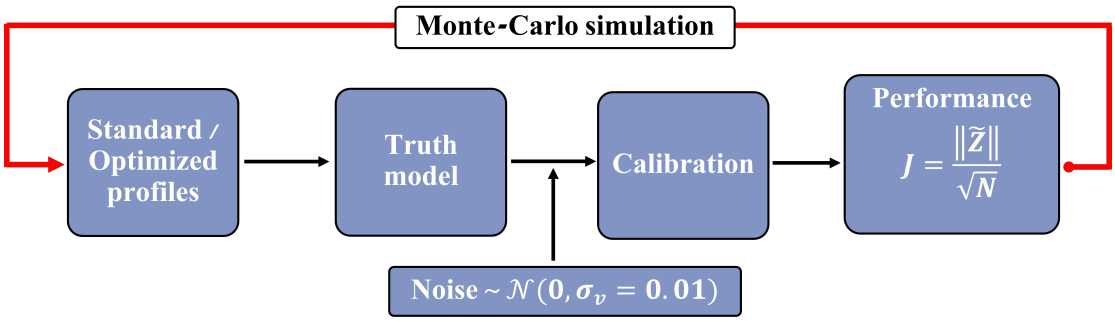

Figure 14. Monte-Carlo simulation flow chart.

3. Results

The results are summarized in Tables VI.B.3 and IX. The expected least-squares costs from Monte-Carlo simulations are significantly lower in the "novel" approach when compared to the "standard" approach, see Table VI.B.3. Notice that the differences appear when testing the calibration with the reference profiles, while the results are very close when testing on the calibration profiles. Additional insights rose by examining the estimation error covariance matrices. Breaking down the error sources as biases, scale-factors (SF), their nonlinearities (NL), and misalignament/nonorthogonality (MANO), one can check the variances of each estimation error, see TableIX. All estimation errors are lower with the novel approach when compared to the standard approach, except for the bias term that is temperature independent. For further comparison the estimation error variances produced by the optimal profiles from the randomized approach have been calculated, too. The novel approach appear to be suboptimal of course and one can evaluate what might still be gained by refining the input profiles.

DOI: 10.13009/EUCASS2022-7272

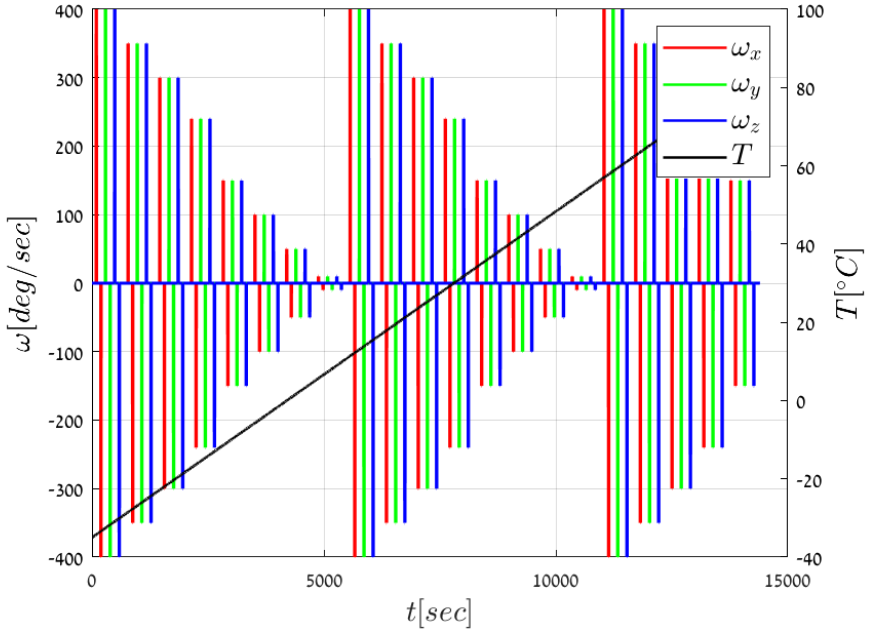

Figure 15. Standard measurement profiles for T and ω.

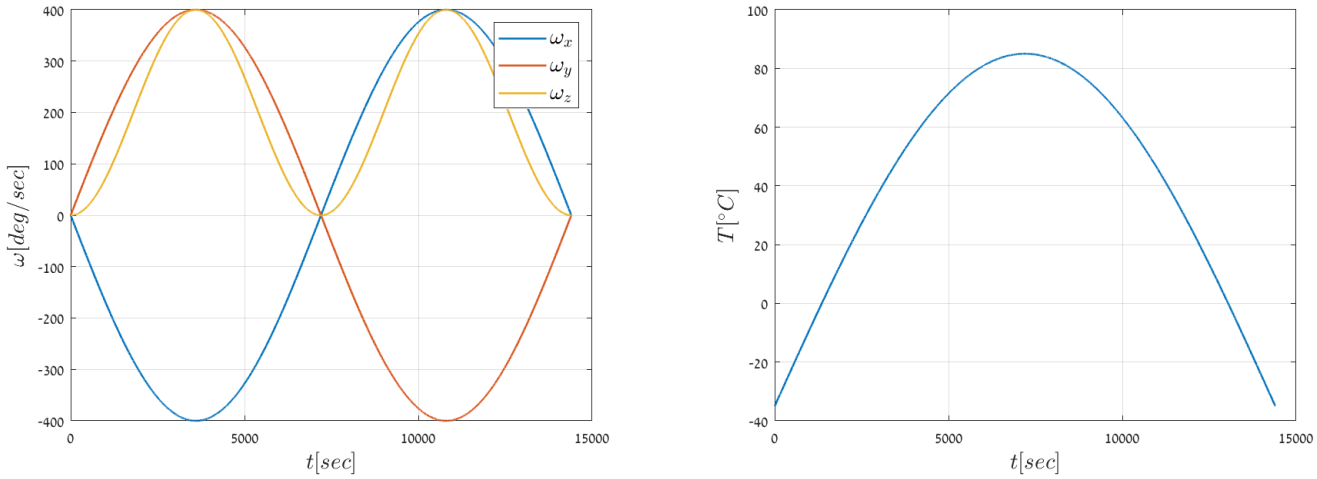

Figure 16. Reference set 1. ω and T profiles.

$J_{MC}\,[\frac{deg}{sec}]$	standard system	novel system	improvement [%]
same set	0.0100	0.0100	–
reference set 1	0.0112	0.0101	92
reference set 2	0.0116	0.0101	94
reference set 3	0.0114	0.0101	93

Table 6. Simulated calibration results. $\mathbf{N}_{MC} = 200$.

DOI: 10.13009/EUCASS2022-7272

explanation to the novel better results:

As can be seen in the following figures, both histograms of the calibration sets, both the standard and novel, are presented. It's pretty obvious that the novel calibration set has much similar distribution, like the one from the optimal calibration

the variance was calculated as follow:

$$\sigma_{\omega^m} = \sqrt{HP_{\tilde{x}}H^T + R} \tag{99}$$

The following plot described the standard deviation for the x axis, in the case both $\omega_y = \omega_z = 0$, which represent only the bias, SF and NL variance.

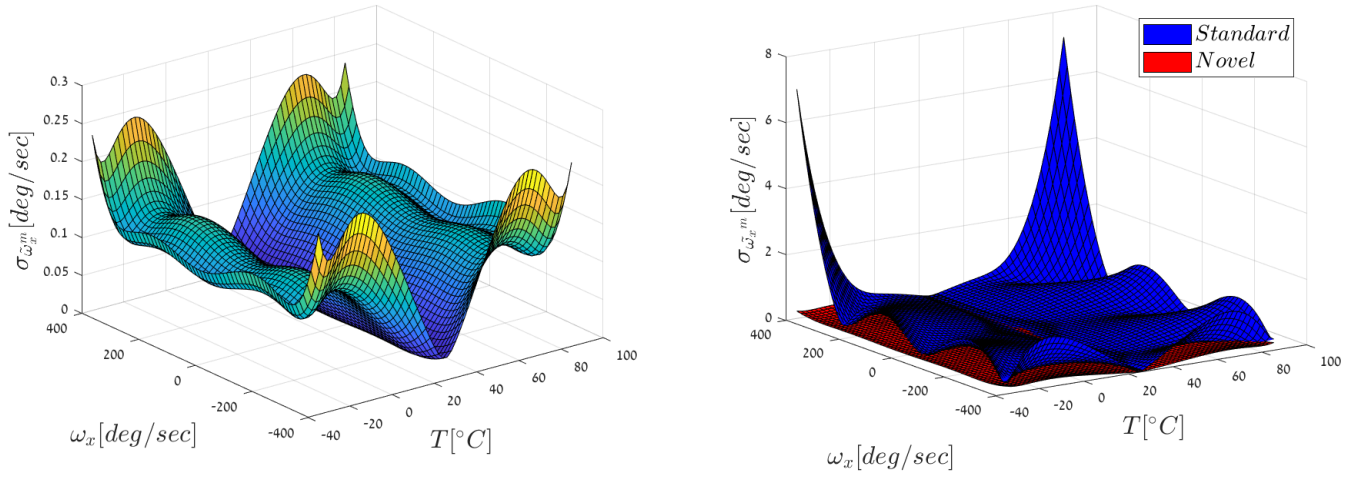

Figure 17. Measurement std analysis in both the novel and a comparison

In order to exam the results, a Monte-Carlo simulation, using the Truth model, was preformed in order to recrate the following surface.

$$\sigma_{\omega^m} = \sqrt{(z_{truth} - H\hat{x})^2} \tag{100}$$

Notice, the white noise term was subtract from the calculation in order to emphasis the results. Both surface seems the same as the ones calculates from the deterministic case,using the covariance, and the residual error from the novel method is still better than the standard.

also, it is possible to try and separate the influence of the error source,using sum matrix that relevent to the error.

$$\sigma_{\omega^m} = \sqrt{hp_{\tilde{x}}h} \tag{101}$$

where h and p are sub matrices of H and P respectively.For example, in the SF case in x axis, p is a 4x4 matrix include the SF variance and correlation,and h is as follow:

$$\text{h}= \left[\omega_x \, \omega_x T \, \omega_x T^2 \, \omega_x T^3\right]_{1\times 4}$$

DOI: 10.13009/EUCASS2022-7272

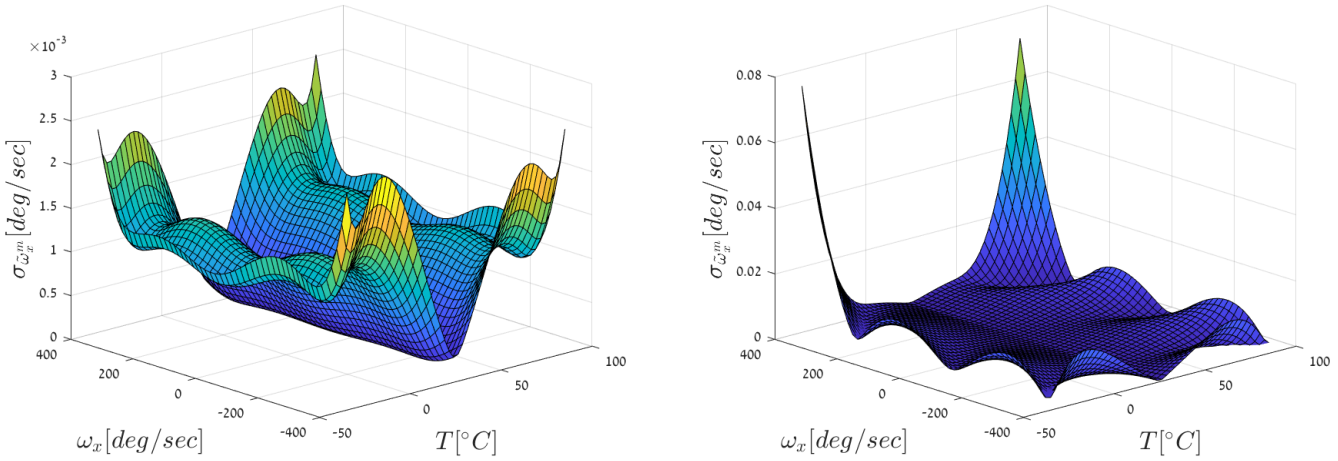

Figure 18. Measurement std in Monte-Carlo simulation. novel(left) and standard(right) $\mathbf{N}_{MC} = 200$

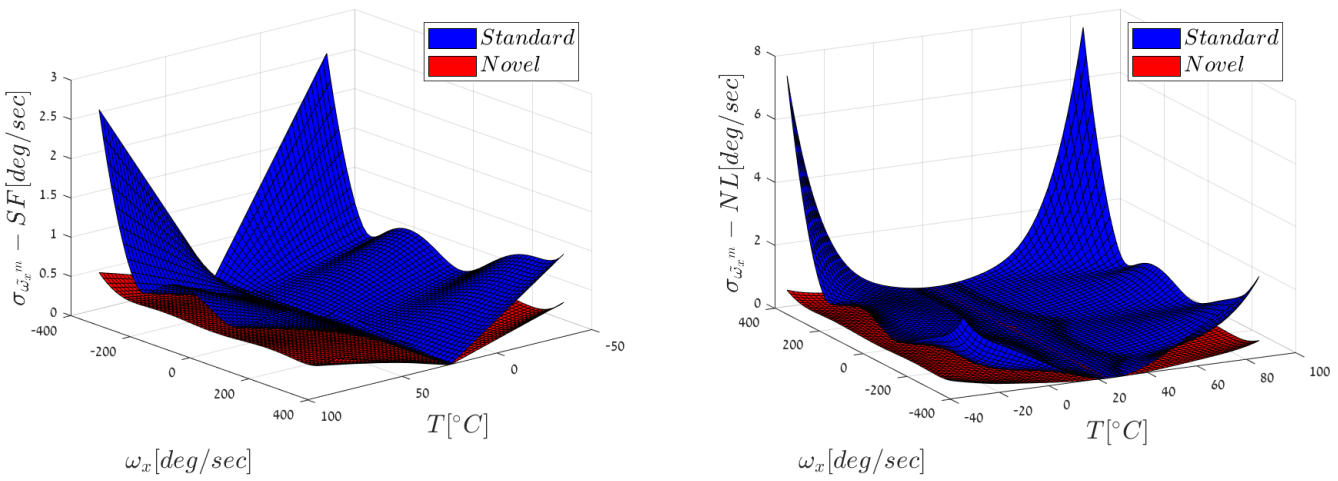

Figure 19. std comparison for SF (left) and NL (right)

the following figures present the results:

As can be seen, the results for the novel calibration outperform the standard calibration except from the bias, which which depended on the temperature we are comparing at.

C. Experimental calibration

An experiment was conducted on a calibration table using an IMU with Silicon Sensing MEMS vibrating ring gyros of CRM100 type. The experiment lasted 2.5 hours. Due to operational limitations, the temperature profile could not follow the desired piecewise linear profile or span the desired range. The sampled values of the angular rates were

DOI: 10.13009/EUCASS2022-7272

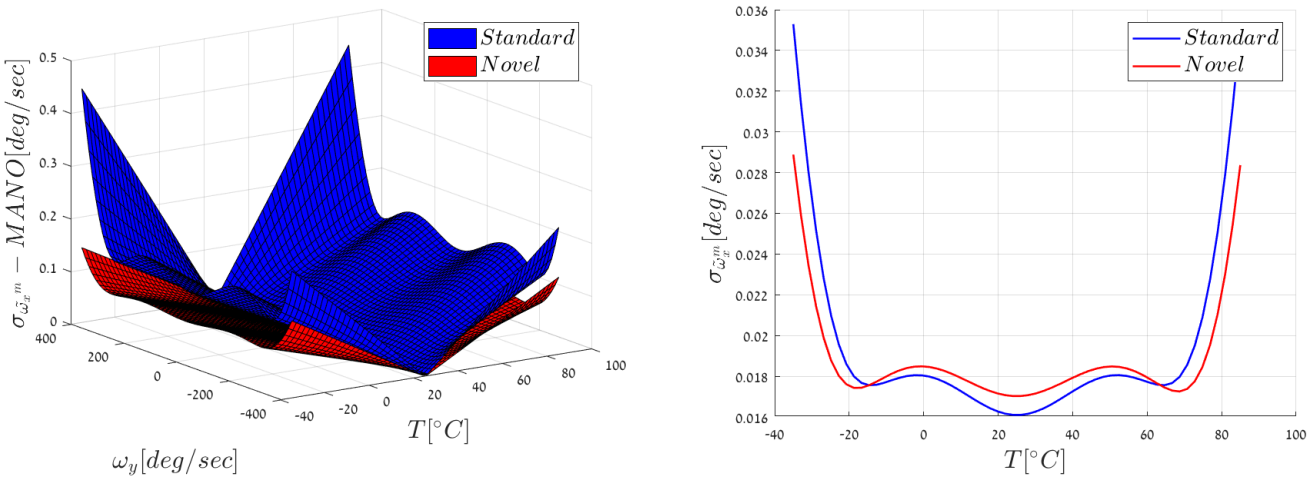

Figure 20. std comparison for MANO (left) and bias (right)

$\pm 150, \pm 240, \pm 300, \pm 400, [deg/sec]$. The input profiles of ω and T are depicted in Figure 21. Half of the measurements was used for the calibration. The calibration set is shown in Figure 22. It includes the angular rates $\pm 400, \pm 240 [deg/sec]$. The other half of the measurements was used for the validation. It includes the rates $\pm 150, \pm 300 [deg/sec]$. Figure 23 depicts the performances in the angular rates estimation for each level and for various values of the temperature. The circles show the values of the root of squares of the errors in the three axes, while the bars depict the spans of the errors for all three axes. The errors are shown in *ppm*: for instance the novel method produces an error of 100 ppm versus 700 ppm for the standard calibration, at $T = 7^o C$ for a rate of 300 $[deg/sec]$. At $\omega = \pm 300 [deg/sec]$, the novel method produces estimation errors that oscillate between 50 and 150 ppm, with very narrow spans, while the standard method's errors are up to 650 ppm. The difference is narrower at $\omega = \pm 150 [deg/sec]$ with gaps of 50 ppm between both methods. Nevertheless, the difference is consistently to the advantage of the novel method, except for a narrow range of high temperatures at $\omega = \pm 100 [deg/sec]$ where their results are comparable. The spans also show that the novel method is producing errors with smaller deviations. A remarkable result from the novel method is that the errors and the spans are not very sensitive to the temperature. On the other hand the standard method shows a very clear trend where the errors and their spans grow as the temperature decreases. The largest gaps among both methods appear around $T = 7^o C, 10^o C$. Whether this trend would reverse as T becomes negative and decreases to its lower bound remains to be tested in a subsequent experiment, but the current results already illustrate how the novel method outperforms a standard calibration. Another maybe more convenient way to display the performances is to consider the breakdown of the angular rate estimation error per biases, scale-factors and their nonlinearities (SF/NL), and misalignment nonorthogonality (MANO). This is shown in Table VI.C. All values are in deg/sec and depict the square-root second-order moments of the associated errors produced from the experimental sample. The novel method displays biases that are three-fold lower, MANO errors that are lower by at least one order of magnitude, and SF/NL compound errors that are mostly smaller compared with the standard method. Notice that these performances are calculated over the range of temperatures and angular rates variations.

DOI: 10.13009/EUCASS2022-7272

Error term	parameter	standard system	novel system	optimal result
Bias	$b_{x0}\frac{deg}{sec}$	$2.251e-04$	$2.416e-04$	$4.073e-04$
	$b_{x1}\frac{deg}{sec^\circ C}$	$2.191e-06$	$1.969e-06$	$2.359e-07$
	$b_{x2}\frac{deg}{sec^\circ C^2}$	$4.362e-10$	$3.253e-10$	$2.823e-10$
	$b_{x3}\frac{deg}{sec^\circ C^3}$	$6.630e-14$	$4.831e-14$	$4.094e-14$
SF	β_{x0}	$2.365e-06$	$3.837e-07$	$7.659e-08$
	$\beta_{x1}\frac{1}{^\circ C}$	$3.329e-09$	$3.455e-10$	$4.299e-11$
	$\beta_{x2}\frac{1}{^\circ C^2}$	$1.400e-11$	$5.554e-13$	$5.193e-14$
	$\beta_{x3}\frac{1}{^\circ C^3}$	$1.198e-15$	$8.393e-17$	$7.573e-18$
NL	$\gamma_{x0}\frac{sec}{deg}$	$7.356e-11$	$6.557e-12$	$1.519e-12$
	$\gamma_{x1}\frac{sec}{deg^\circ C}$	$4.860e-14$	$5.954e-15$	$8.566e-16$
	$\gamma_{x2}\frac{sec}{deg^\circ C^2}$	$3.356e-16$	$9.498e-18$	$1.033e-18$
	$\gamma_{x3}\frac{sec}{deg^\circ C^3}$	$3.276e-20$	$1.437e-21$	$1.505e-22$
	$\delta_{x0}\frac{sec^2}{deg^2}$	$8.425e-17$	$2.061e-17$	$3.886e-18$
	$\delta_{x1}\frac{sec^2}{deg^2\circ C}$	$5.332e-19$	$1.715e-20$	$2.181e-21$
	$\delta_{x2}\frac{sec^2}{deg^2\circ C^2}$	$3.039e-22$	$2.937e-23$	$2.630e-24$
	$\delta_{x3}\frac{sec^2}{deg^2\circ C^3}$	$3.452e-26$	$4.400e-27$	$3.849e-28$
	$\alpha_{x0}\frac{sec^3}{deg^3}$	$1.761e-21$	$2.889e-22$	$6.084e-23$
	$\alpha_{x1}\frac{sec^3}{deg^3\circ C}$	$9.002e-24$	$2.534e-25$	$3.424e-26$
	$\alpha_{x2}\frac{sec^3}{deg^3\circ C^2}$	$7.321e-27$	$4.158e-28$	$4.131e-29$
	$\alpha_{x3}\frac{sec^3}{deg^3\circ C^3}$	$5.999e-31$	$6.264e-32$	$6.027e-33$
MA	m_{xy0}	$1.814e-07$	$4.253e-08$	$1.814e-09$
	$m_{xy1}\frac{1}{^\circ C}$	$1.385e-10$	$3.490e-11$	$1.385e-12$
	$m_{xy2}\frac{1}{^\circ C^2}$	$2.809e-13$	$5.748e-14$	$2.809e-15$
	$m_{xy3}\frac{1}{^\circ C^3}$	$6.160e-17$	$8.361e-18$	$6.160e-19$
	m_{xz0}	$1.857e-07$	$3.899e-08$	$1.857e-09$
	$m_{xz1}\frac{1}{^\circ C}$	$1.257e-10$	$3.615e-11$	$1.257e-12$
	$m_{xz2}\frac{1}{^\circ C^2}$	$3.211e-13$	$4.862e-14$	$3.211e-15$
	$m_{xz3}\frac{1}{^\circ C^3}$	$6.160e-17$	$7.080e-18$	$6.160e-19$

Table 7. Simulated calibration results. Estimation error variances.

Term	standard system	novel system
Bias	13.24	28.26
SF	$5.54e-05$	0.0138
NL	$1.08e-20$	$2.638e-10$
MA	$2.495e-11$	$1.892e-06$

Table 8. Det results, all the values are in percentage reletive to the optimal result.

DOI: 10.13009/EUCASS2022-7272

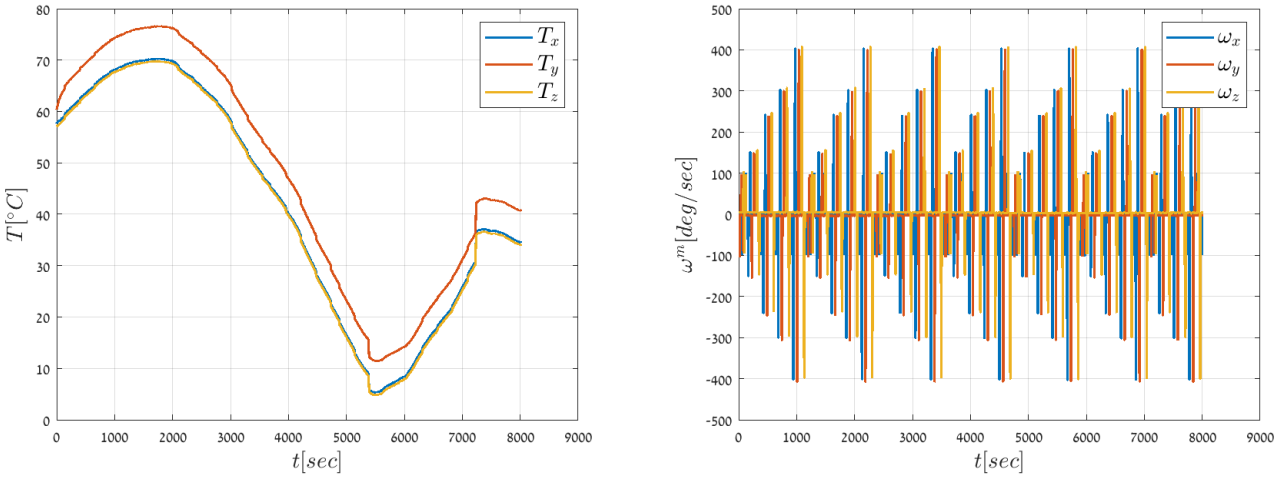

Figure 21. Experience. Input profiles for T and ω.

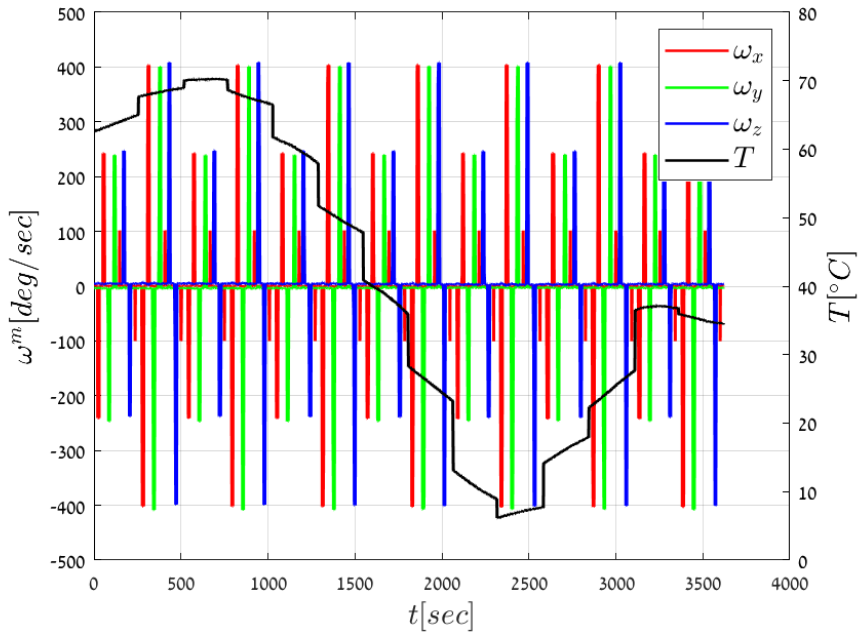

Figure 22. Experience. Calibration set for T and ω.

DOI: 10.13009/EUCASS2022-7272

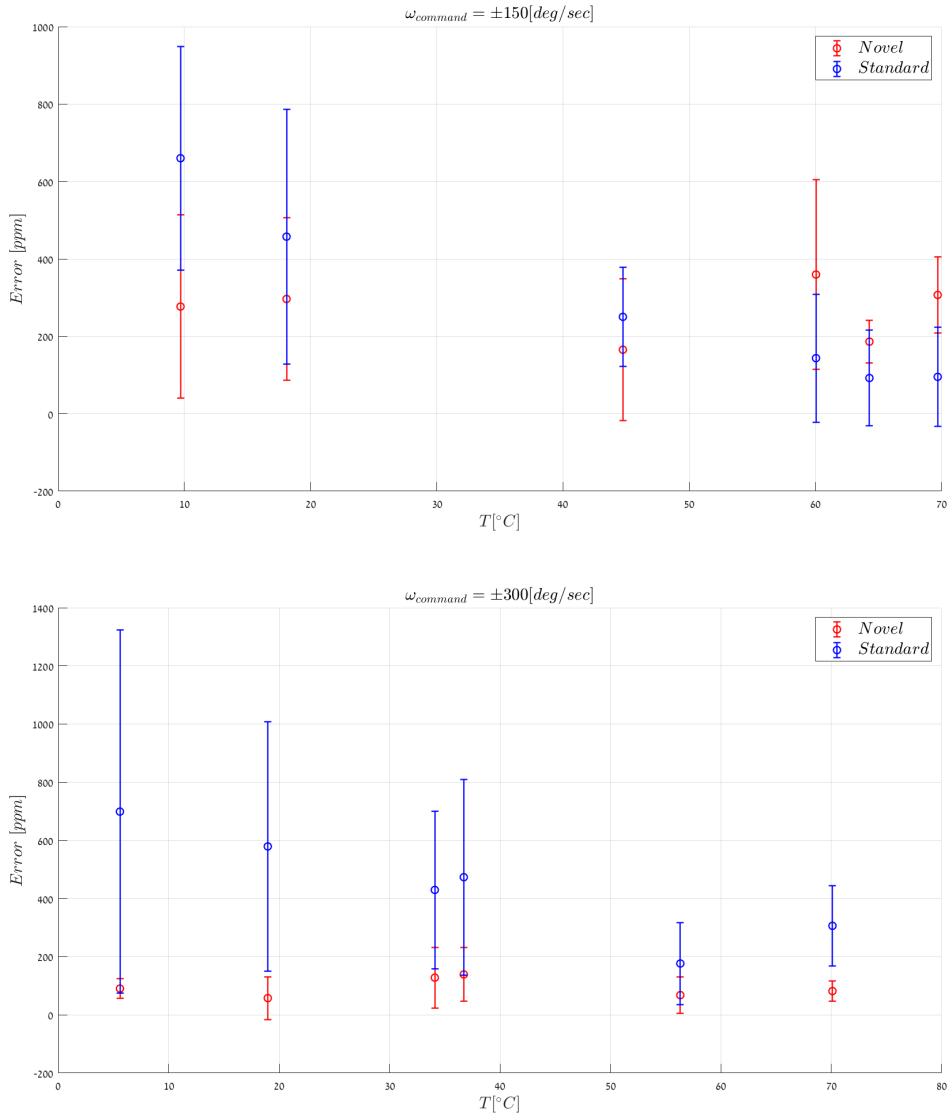

Figure 23. Experience. Validation using $\omega = \pm 150, \pm 300[deg/sec]$**.**

VII. Accelerometers calibration: simulation and experiment

A. Measurement model

The truth and design measurement models for the accelerometers are identical. Formally they are similar to the gyro rate measurement model, albeit with different assumptions.

$$\begin{pmatrix} a_x^m \\ a_y^m \\ a_z^m \end{pmatrix} = \begin{pmatrix} b_x \\ b_y \\ b_z \end{pmatrix} + \begin{bmatrix} \beta_x & \psi_{xy} & \psi_{xz} \\ \psi_{yx} & \beta_y & \psi_{yz} \\ \psi_{zx} & \psi_{zy} & \beta z \end{bmatrix} \begin{pmatrix} a_x \\ a_y \\ a_z \end{pmatrix} + \begin{pmatrix} \epsilon_x \\ \epsilon_y \\ \epsilon_z \end{pmatrix} \tag{102}$$

where
a_x^m, a_y^m, a_z^m: measured accelerations
a_x, a_y, a_z: true acceleration, known through the table commanded position
b_x, b_y, b_z: biases

DOI: 10.13009/EUCASS2022-7272

component	axis	standard	novel
Bias	x	0.0335	0.0188
	y	0.0465	0.0197
	z	0.0752	0.0209
SF/NL	x	0.0233	0.0149
	y	0.0859	0.0170
	z	0.0076	0.0167
MANO	x	0.1950	0.0023
	y	0.3245	0.0193
	z	0.3310	0.0077

Table 9. Experiment. Angular rate error breakdown. Square-root of the second-order moments from the experimental samples. All values in $[deg/sec]$

$\beta_x, \beta_y, \beta_z$: scale factors that are independent of $\mathbf{a}$
$\epsilon_x, \epsilon_y, \epsilon_z$: independent identically distributed noise terms.
Each of the biases and SF parameters allocated to each axis is assumed to vary with the temperature according to a third order polynomial, as follows:

$$b = b_0 + b_1 T + b_2 T^2 + b_4 T^3 \tag{103}$$

$$\beta = \beta_0 + \beta_1 T + \beta_2 T^2 + \beta_3 T^3 \tag{104}$$

and the MA parameters are assumed to be constant. There are 10 parameters per axis, hence 30 parameters for the three axes. Notice the similarity of the accelerometer equation with that of the rate gyroscope. Given that the constraints are similar as well, we expect that the design optimization will yield similar results, which is indeed the case. For the sake of brevity we do not provide more development in this report. As a result, we simply opt to use the design of the temperature obtained in the previous section. The sampling design problem of the accelerations levels is following a standard approach that consists of building a sequence that periodically aligns all accelerometer axes with the local vertical, as shown in Fig. 24.

B. Methodology

The calibration process consists of a least-squares batch estimator. Two performance indices are defined, one related to the estimation errors, the other with respect to the measurement residuals, as follows:

$$J^p = \sqrt{\sum_{i=1}^{30} \left(\frac{i}{x_i} \right)^2} \tag{105}$$

where $_i$ denotes the estimation error in the ith parameter. Another cost index is defined from the residuals themselves:

$$J^z = \frac{\|Z\|}{\sqrt{N}} \tag{106}$$

DOI: 10.13009/EUCASS2022-7272

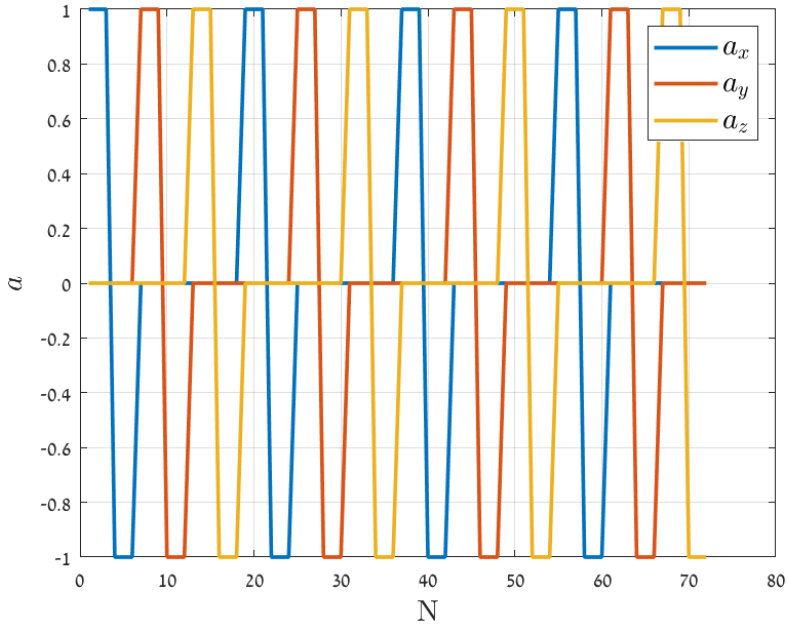

Figure 24. Accelerations profile.

where Z is an $N \times 1$ vector of acceleration measurements. As done in the gyro case, these indices will be calculated using either the same data or reference data. Also, Monte-Carlo averages of the costs will be calculated by running N_{MC} sequences of noises. Figure 25 depicts a particular set of reference data.

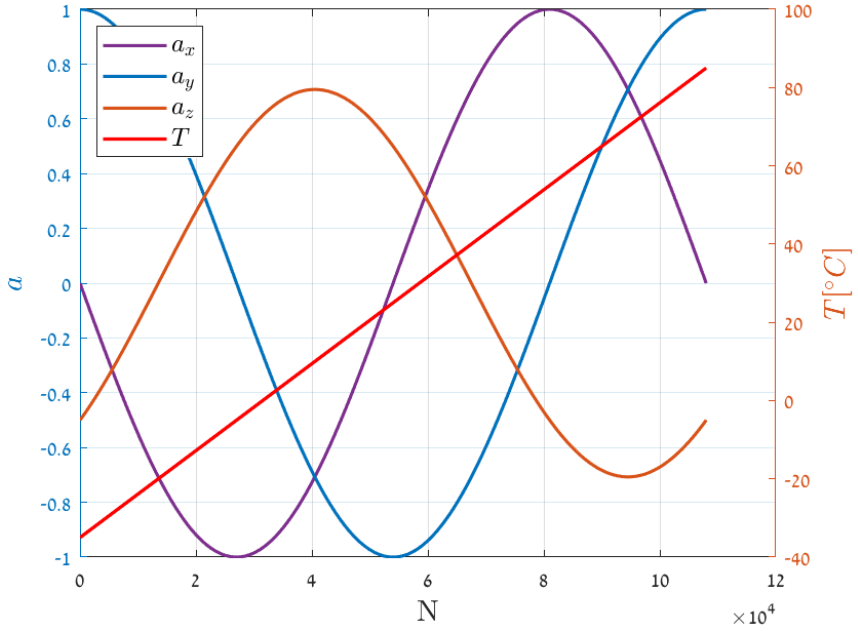

Figure 25. Reference accelerations and temperature profiles.

DOI: 10.13009/EUCASS2022-7272

C. Results

An experiment was performed on a set of three SAFRAN MS9000 MEMS capacitive accelerometers. The simulated and experimental calibration results are summarized in Table VII.C.

	Novel set	Standard set
J^P_{MC}	0.3155	0.3202
J^Z_{MC} - same set	0.01	0.01
J^Z_{MC} - reference set 1	0.01	0.01
J^Z_{MC} - reference set 2	0.01	0.01
J^Z_{MC} - reference set 3	0.01	0.01

Table 10. Accelerometers. Simulated and experimental calibration results. N = 54,000 samples. $\mathbf{N}_{MC} = 100 runs.$

D. Concluding remarks

The calibration of the accelerometers shows that the proposed temperature profile along with a standard sequence for the accelerations measurements yields better performances in the estimation errors. On the other hand the residuals Monte-Carlo averages remain identical among all the test cases. This is indeed expected since the unweighted least-squares cost is not sensitive to the measurement schedule when both design and truth models are identical.

VIII. Conclusion

An optimization-based approach for IMU calibration is proposed in this work. The efficiency of the proposed methodology was illustrated via a proof-of-concept verification and validation test case. In particular, errors in the gyroscopes measurement output can be improved several-folds up to one order of magnitude. Yet the theory also carries limitations: if the design and the truth models are identical the least-squares cost becomes insensitive to the input profiles. The widespread case of model mismatch, however, ensures that the proposed optimization should find useful applications.

IX. Appendix

The values of the Truth model for the three-axes gyroscope are and three-axes accelerometer are given below.

DOI: 10.13009/EUCASS2022-7272

Error term	parameter	x	y	z
Bias	$b_0 \frac{deg}{sec}$	0.020	-0.159	0.0197
	$b_1 \frac{deg}{sec^\circ C}$	$2.130e-03$	$1.490e-03$	$2.940e-03$
	$b_2 \frac{deg}{sec^\circ C^2}$	$-2.480e-04$	$1.430e-04$	$-1.770e-04$
	$b_3 \frac{deg}{sec^\circ C^3}$	$4.050e-07$	$-1.520e-07$	$1.160e-07$
SF	β_0	0.975	0.965	0.985
	$\beta_1 \frac{1}{^\circ C}$	$-1.080e-03$	$9.420e-04$	$-1.990e-03$
	$\beta_2 \frac{1}{^\circ C^2}$	$8.120e-06$	$1.340e-05$	$7.550e-06$
	$\beta_3 \frac{1}{^\circ C^3}$	$4.440e-06$	$-4.413e-07$	$-7.350e-07$
NL	K	0.56	0.58	0.54
	$S_{10} \frac{deg}{sec}$	-21.060	-20.060	-22.050
	$S_{11} \frac{deg}{sec^\circ C}$	$1.000e-04$	$0.960e-04$	$1.100e-04$
	$S_{12} \frac{deg}{sec^\circ C^2}$	$2.000e-06$	$2.200e-06$	$1.900e-06$
	$S_{20} \frac{deg}{sec}$	-0.932	-0.964	-0.912
	$S_{30} \frac{deg}{sec}$	0.112	0.108	0.124
	$S_{40} \frac{deg}{sec}$	0.027	0.031	0.023
	$C_{10} \frac{deg}{sec}$	-2.500	-2.550	-2.450
	$C_{11} \frac{deg}{sec^\circ C}$	$5.000e-05$	$4.500e-05$	$5.200e-05$
	$C_{20} \frac{deg}{sec}$	-0.240	-0.270	-0.250
	$C_{30} \frac{deg}{sec}$	0.227	0.212	236
	$C_{40} \frac{deg}{sec}$	-0.045	-0.040	-0.042
MA	m_{ij0}	0.012	-0.011	-0.013
	$m_{ij1} \frac{1}{^\circ C}$	$1.385e-04$	$3.490e-04$	$1.385e-04$
	$m_{ij2} \frac{1}{^\circ C^2}$	$2.809e-06$	$5.748e-06$	$2.809e-06$
	$m_{ij3} \frac{1}{^\circ C^3}$	$6.160e-08$	$8.361e-08$	$6.160e-08$
	m_{ik0}	0.010	0.015	0.014
	$m_{ik1} \frac{1}{^\circ C}$	$1.257e-04$	$3.615e-04$	$1.257e-04$
	$m_{ik2} \frac{1}{^\circ C^2}$	$3.211e-06$	$4.862e-06$	$3.211e-06$
	$m_{ik3} \frac{1}{^\circ C^3}$	$6.160e-08$	$7.080e-08$	$6.160e-08$

Table 11. Truth Model Parameters for the three axes gyroscope simulated calibration.

DOI: 10.13009/EUCASS2022-7272

Error term z	parameter	units	x	y
Bias	$b_0 \frac{deg}{sec}$	0.0827	-0.112	0.0486
	$b_1 \frac{deg}{sec^\circ C}$	$5.1233e-04$	$-8.809e-05$	0.0013
	$b_2 \frac{deg}{sec^\circ C^2}$	$-1.2132e-05$	$6.997e-06$	$-7,982e-06$
	$b_3 \frac{deg}{sec^\circ C^3}$	$-1.1771e-08$	$1.505e-08$	$1.8386e-09$
SF	β_0	0.9993	0.9992	0.9992
	$\beta_1 \frac{1}{^\circ C}$	$-1.012e-04$	$-1.188e-04$	$-8.421e-05$
	$\beta_2 \frac{1}{^\circ C^2}$	$8.472e-07$	$3.975e-07$	$3.063e-07$
	$\beta_3 \frac{1}{^\circ C^3}$	$-4.41663e-09$	$1.517e-09$	$1.447e-09$
MA	m_{ij0}	-0.0139	0.005	-0.0112
	m_{ik0}	0.0133	0.001	0.0086

Table 12. Truth Model Parameters for the three axes accelerometer simulated calibration.

DOI: 10.13009/EUCASS2022-7272

References

1. C. Fan, Z. Jin, W. Tian, F. Qian, Temperature drift modelling of fiber optic gyroscopes based on a grey radial basis function neural network, *Meas. Sci. Technol.*, 15, 119, 2004.

2. P. Aggarwal, Z. Syed, X. Niu, N. El-Sheymi, Cost-effective Testing and Calibration of Low Cost MEMS Sensors for Integrated Positioning, Navigation and Mapping Systems, *XXIII FIG Congress*, Munich, Germany, 2006.

3. M. El-Diasty, A. El-Rabbany, S. Pagiatakis, Temperature variation effects on stochastic characteristics for low-cost MEMS-based inertial sensor error, *Meas. Sci. Technol.*, 18, 2007.

4. G. Xu, W. Tian, L. Qian, EMD- and SVM-based temperature drift modeling and compensation for a dynamically tuned gyroscope (DTG), *Meas. Sci. Technol.*, 21, 2007.

5. M. El-Diasty, S. Pagiatakis, A Rigorous Temperature-Dependent Stochastic Modelling and Testing for MEMS-Based Inertial Sensor Errors, *Sensors*, 9, 2009.

6. Z. Zhixiong, F. Lihui, S. Yu-nan, Temperature Modeling and Compensation of Double H Quartz Tuning Fork Gyroscope, *Procedia Engineering*, 15, 2011.

7. Z. Berman, Inertial Sensors-A New Approach for Low Cost Calibration and Testing. *Proceedings of Inertial Sensors and Systems*, Karlsruhe, Germany, 2011.

8. J.-K. Shiau, C.-X. Huang, M.-Y. Chang, Noise Characteristics of MEMS Gyros Null Drift and Temperature Compensation, *Journal of Applied Science and Engineering*, Vol. 15, No. 3, 2012.

9. Z. Berman, Inertial Sensors: Further Developments in Low-Cost Calibration and Testing. *In Proceedings of IEEE/ION Position Location and Navigation Symposium (PLANS)*, Myrtle Beach, SC, USA, April 2012.

10. X. Niu, Y. Li, H. Zhang, Q. Wang, Y. Ban, Fast Thermal Calibration of Low-Grade Inertial Sensors and Inertial Measurement Units, *Sensors*, 2013.

11. X. Chen, R. Song, C. Shen, H. Zhang, Application of a genetic algorithm Elman network in temperature drift modeling for a fiber-optic gyroscope, *Applied Optics*, Vol. 53, No. 26, 2014.

12. C. Shen, R. Song, J. Li, X. Zhang, J. Tang, Y. Shi, J. Liu, H. Cao, Temperature drift modeling of MEMS gyroscope based on genetic-Elman neural network, *Mechanical Systems and Signal Processing*, 72-73, 2016.

13. C. Shen, J. Li, X. Zhang, J. Tang, H. Cao, J. Liu, Multi-scale parallel temperature error processing for dual-mass MEMS gyroscope, *Sensors and Actuators A*, 245, 2016.

14. B. Zhang, H. Chu, T. Sun, L. Guo, Thermal calibration of a tri-axial MEMS gyroscope based on Parameter-Interpolation method, *Sensors and Actuators A: Physical*, 261, 2017.

15. R. Fontanella, D. Accardo, R. S. Lo Moriello, L. Angrisani, D. De Simone, MEMS gyros temperature calibration through artificial neural networks, *Sensors and Actuators A: Physical*, 279, 2018.

16. W.F. Denham, J.L. Speyer, Optimal measurement and velocity correction programs for midcourse guidance, *AIAA Journal*, Vol 5, No. 2, 1964.

17. V. V. Fedorov, Theory of Optimal Experiments. New York, NY, USA: Academic, ch. 2. 1972.

DOI: 10.13009/EUCASS2022-7272

18. R. Mehra, Optimization of measurement schedules and sensor designs for linear dynamic systems,*IEEE Trans. Automat. Control*, vol. 21, no. 1, 1976.

19. Y. Oshman, P. Davidson, Optimization of observer trajectories for bearings-only target localization, *IEEE Transactions on Aerospace and Electronic Systems*, vol. 35, no. 3, 1999.

20. L. Ljung, System Identification: Theory for the User, *Prentice Hall*, Chap. 13, 1999.

21. M. Salvoldi and D. Choukroun, Process Noise Covariance Design in Kalman Filtering via Bounds Optimization, *IEEE Transactions on Automatic Control*, vol. 64, no. 2, 2019.

22. A.E. Bryson, Y.-C. Ho, Applied Optimal Control, *Blaisdell Publishing Company*, Chap. 1, 1969.